Divergence of Ca^{2+} selectivity and equilibrium Ca^{2+} blockade in a Ca^{2+} release-activated Ca^{2+} channel

Megumi Yamashita and Murali Prakriya

Department of Molecular Pharmacology and Biological Chemistry, Northwestern University Feinberg School of Medicine, Chicago, IL 60611

Prevailing models postulate that high Ca^{2+} selectivity of Ca^{2+} release-activated Ca^{2+} (CRAC) channels arises from tight Ca^{2+} binding to a high affinity site within the pore, thereby blocking monovalent ion flux. Here, we examined the contribution of high affinity Ca^{2+} binding for Ca^{2+} selectivity in recombinant Orai3 channels, which function as highly Ca^{2+}-selective channels when gated by the endoplasmic reticulum Ca^{2+} sensor STIM1 or as poorly Ca^{2+}-selective channels when activated by the small molecule 2-aminoethoxydiphenyl borate (2-APB). Extracellular Ca^{2+} blocked Na^+ currents in both gating modes with a similar inhibition constant (K_i; ~25 µM). Thus, equilibrium binding as set by the K_i of Ca^{2+} blockade cannot explain the differing Ca^{2+} selectivity of the two gating modes. Unlike STIM1-gated channels, Ca^{2+} blockade in 2-APB–gated channels depended on the extracellular Na^+ concentration and exhibited an anomalously steep voltage dependence, consistent with enhanced Na^+ pore occupancy. Moreover, the second-order rate constants of Ca^{2+} blockade were eightfold faster in 2-APB–gated channels than in STIM1-gated channels. A four-barrier, three–binding site Eyring model indicated that lowering the entry and exit energy barriers for Ca^{2+} and Na^+ to simulate the faster rate constants of 2-APB–gated channels qualitatively reproduces their low Ca^{2+} selectivity, suggesting that ion entry and exit rates strongly affect Ca^{2+} selectivity. Noise analysis indicated that the unitary Na^+ conductance of 2-APB–gated channels is fourfold larger than that of STIM1-gated channels, but both modes of gating show a high open probability (P_o; ~0.7). The increase in current noise during channel activation was consistent with stepwise recruitment of closed channels to a high P_o state in both cases, suggesting that the underlying gating mechanisms are operationally similar in the two gating modes. These results suggest that both high affinity Ca^{2+} binding and kinetic factors contribute to high Ca^{2+} selectivity in CRAC channels.

INTRODUCTION

Ca^{2+} is a multifunctional signaling messenger crucial for diverse biological processes. Among the various ways by which cellular Ca^{2+} signals are generated, store-operated Ca^{2+} release-activated Ca^{2+} (CRAC) channels are recognized as a widespread mechanism for regulating transcription, motility, and proliferation in many cells (Feske, 2009; Hogan et al., 2010; Lewis, 2011). CRAC channels produce sustained intracellular Ca^{2+} elevations and are implicated in a growing list of human diseases including immunodeficiency (Feske, 2009), allergy (Di Capite et al., 2011), cancer (Prevarskaya et al., 2011), thrombosis (Varga-Szabo et al., 2011), and inflammatory bowel disease (McCarl et al., 2010). The broad expression of CRAC channels and their involvement in many physiological processes has produced intense interest in CRAC channels as targets for drug development. Yet, our understanding of how CRAC channels operate at a mechanistic level is still rudimentary and, in particular, the molecular and structural mechanisms of ion permeation and channel gating are only now beginning to be elucidated.

A distinguishing feature of CRAC channels is high Ca^{2+} selectivity ($P_{Ca}/P_{Na} \approx 1{,}000$; Hoth and Penner, 1993). Current thinking about the origin of this selectivity is rooted in the idea of preferential Ca^{2+} binding to a high affinity binding site ($K \approx 20$ µM) at the selectivity filter, which occludes Na^+ flux through the pore (Prakriya, 2009). In support of this idea, a mutation at the predicted CRAC channel selectivity filter (E106D in Orai1) diminishes both Ca^{2+} selectivity as well as the affinity of Ca^{2+} blockade of Na^+ flux (Prakriya et al., 2006; Vig et al., 2006; Yeromin et al., 2006; Yamashita et al., 2007), which would be expected if Ca^{2+} selectivity is primarily determined by the K_i of Na^+ current blockade. Such a selection-through-affinity mechanism was originally described for voltage-gated Ca^{2+} channels, which, like CRAC channels, display exquisite Ca^{2+} selectivity ($P_{Ca}/P_{Na} >$ 1,000; Sather and McCleskey, 2003). However, the apparent affinity of Ca^{2+} block is roughly 20-fold higher in voltage-gated Ca^{2+} channels than CRAC channels (K_d of ~1 vs. 20 µM, respectively; Almers and McCleskey, 1984; Bakowski and Parekh, 2002; Su et al., 2004; Prakriya and

Correspondence to Murali Prakriya: m-prakriya@northwestern.edu

Abbreviations used in this paper: 2-APB, 2-aminoethoxydiphenyl borate; CRAC, Ca^{2+} release-activated Ca^{2+}; DVF, divalent-free; P_o, open probability.

The Rockefeller University Press $30.00
J. Gen. Physiol. Vol. 143 No. 3 325–343
www.jgp.org/cgi/doi/10.1085/jgp.201311108

Lewis, 2006), raising the possibility that the biophysical mechanisms of how these channels achieve high Ca^{2+} selectivity may differ. Importantly, although appealing in its simplicity, it remains uncertain whether an equilibrium binding model fully explains how CRAC channels achieve Ca^{2+} selectivity under physiological nonequilibrium conditions.

A convenient CRAC channel system in which this and related questions of ion selectivity can be investigated is the Orai3 channel. When overexpressed in HEK293 cells, Orai3 channels produce either Ca^{2+}-selective or nonselective currents, depending on whether they are activated by the ER Ca^{2+} sensor, STIM1, or the small molecule 2-aminoethoxydiphenyl borate (2-APB; DeHaven et al., 2008; Peinelt et al., 2008; Schindl et al., 2008; Zhang et al., 2008; Yamashita et al., 2011). The selection-through-affinity model predicts that Ca^{2+} binding affinity in the poorly selective 2-APB–activated Orai3 channels should be lower, a possibility that is directly tested in this study.

In addition to Ca^{2+} selectivity, much attention has surrounded the gating mechanism of CRAC channels. STIM1 interacts with two distinct sites on each Orai subunit and these interactions contribute both to the accumulation of Orai channels at the ER–plasma membrane junctions and channel gating (Li et al., 2007; Muik et al., 2008; Park et al., 2009; McNally et al., 2013). However, our understanding of how STIM1 binding is coupled to channel gating is only now emerging. Biophysical studies using noise analysis have found that activation of CRAC channels after store depletion occurs through stepwise recruitment of closed channels to a high open probability (P_o) state (Prakriya and Lewis, 2006; Kilch et al., 2013). It is tempting to speculate that in the context of an activation mechanism involving reversible binding of multiple STIM1 molecules to CRAC channels (Li et al., 2010; Hoover and Lewis, 2011), the abrupt opening of single CRAC channels follows the concerted binding of the required number of STIM1 molecules to Orai1. A recent study has suggested 2-APB gating may also occur through a similar mechanism, wherein ligand binding (STIM1 or 2-APB) leads to a series of graded conformational changes culminating in stepwise opening of Orai channels (Amcheslavsky et al., 2013). However, whether 2-APB gating in fact occurs through stepwise channel opening has not been directly examined.

In this study we compared permeation, block, and gating of Orai3 channels activated by 2-APB and STIM1 to gain insights into the biophysical mechanisms that shape ion selectivity and gating of Orai channels. Our results indicate that the distinct Ca^{2+} selectivity of STIM1- and 2-APB–gated channels cannot be explained in terms of equilibrium Ca^{2+} binding at the selectivity filter set as defined by the K_d of Ca^{2+} blockade. Rather, we suggest that the kinetic rates of Ca^{2+} and Na^+ entry/exit contribute to the lower Ca^{2+} selectivity of 2-APB–gated channels. Our results also indicate that despite different ion conduction properties, STIM1- and 2-APB–gated channel activation states exhibit modal gating to a high P_o state, suggesting that the allosteric mechanisms that open the pore in response to ligand binding are operationally similar between the two gating modes. Collectively, these results provide new insights into the mechanisms of ion selectivity and gating in Orai channels.

MATERIALS AND METHODS

Cells

HEK293 cells were grown in medium consisting of 44% Dulbecco's modified Eagle's medium (Corning) and 44% Ham's F12 (Corning), supplemented with 10% fetal calf serum (HyClone), 1% 200 mM glutamine, 1% 5000 U/ml penicillin, and 5,000 µg/ml streptomycin. The cells were maintained in log-phase growth at 37°C in 5% CO_2.

Plasmids and transfections

The CFP-Orai3 plasmids used here have been previously described (Yamashita et al., 2011). Site-directed mutagenesis to generate the indicated Orai3 mutants was performed using the QuickChange site-directed mutagenesis kit (Agilent Technologies) according to the manufacturer's instructions and the results were confirmed by DNA sequencing. Orai3 and STIM1 were cotransfected using Transpass D2 (New England Biolabs, Inc.), with 200 ng Orai3 and 300 ng STIM1 per 12-mm coverslip when coexpressed or 200 ng when CFP-Orai3 was expressed alone.

Solutions

The standard extracellular Ringer's solution contained 130 mM NaCl, 4.5 mM KCl, 20 mM $CaCl_2$, 10 mM D-glucose, and 5 mM Na-HEPES, pH 7.4. The divalent-free (DVF) Ringer's solution contained 150 mM NaCl, 10 mM HEDTA, 1 mM EDTA, and 10 mM HEPES, pH 7.4. pH was adjusted to 7.4 with NaOH or CsOH. 10 mM TEA-Cl was added to all extracellular solutions to prevent contamination from voltage-gated K^+ channels. The standard internal solution contained 135 mM caesium aspartate, 8 mM $MgCl_2$, 8 mM BAPTA, and 10 mM Cs-HEPES, pH 7.2. For experiments examining block of Na^+-I_{CRAC} by Ca^{2+}, $CaCl_2$ was added to the standard DVF solution at the appropriate amount calculated from the MaxChelator software (WEBMAXC 2.10, available at http://www.stanford.edu/~cpatton/webmaxc2.htm). The 300- and 600-µM $[Ca^{2+}]_o$ solutions were made by adding the indicated amount of $CaCl_2$ to a nominally Ca^{2+}-free solution containing 150 mM NaCl and 10 mM HEPES, pH 7.4. For the pore-sizing studies described in Fig. 1 B, the following organic compounds were substituted for sodium methanesulfonate in the external solution: hydroxylamine HCl (NH_2OH-HCl), hydrazine HCl (NH_2NH_2-HCl), methylamine HCl (CH_3NH_2-HCl), dimethylamineHCl ($(CH3)_2NH$-HCl), trimethylamineHCl ($(CH_3)_3N$-HCl), and tetramethylammonium chloride ($(CH_3)_4NCl$). These chemicals were purchased from Sigma-Aldrich. pH was adjusted to 7.4 with NMDG except in the case of hydrazine HCl (pH 6.4) and hydroxylamine HCl (pH 6.2), which were studied at acidic pH to increase the ionized concentration of the test ion.

Patch-clamp measurements

Patch-clamp recordings were performed using an Axopatch 200B amplifier (Molecular Devices) interfaced to an ITC-18 input/output board and an iMac G5 computer (Apple). Currents were filtered at 1 kHz with a 4-pole Bessel filter and sampled at 5 kHz. Stimulation and data acquisition and analysis were performed using routines developed on the Igor Pro platform by R.S. Lewis (Stanford University, Palo Alto, CA). The holding potential was

+30 mV unless otherwise indicated. Two types of stimuli were used: (1) a 100-ms step to –100 mV followed by a 100-ms ramp from –100 to +100 mV usually applied every 1 s and (2) continuous recording holding potential at −100 mV. Current amplitudes were typically analyzed at −100 mV unless indicated otherwise.

Noise analysis

200-ms sweeps were acquired at the rate of 4 Hz at a constant holding potential of −100 mV, digitized at 20 kHz, low-pass filtered using at 10 kHz using the amplifier's built-in Bessel filter, and recorded directly to hard disk. The mean current and variance were calculated from each sweep. For spectral analysis, data were low pass filtered using a 20 Hz Gaussian filter and power spectra were computed from either 256- or 1,024-point segments using a Hamming window (Igor Pro; Wavemetrics) and averaged from 3–10 sweeps.

Data analysis

Unless noted otherwise, all data were corrected for leak currents collected in 20 mM Ca^{2+} + 50–100 µM La^{3+}. Averaged results are presented as the mean value ± SEM at −100 mV unless indicated otherwise. All curve fitting was done by least-squares methods using built-in functions in Igor Pro 5.0. The minimal pore diameter was estimated as previously described (Prakriya and Lewis, 2006; Yamashita et al., 2007). In brief, relative permeabilities to various organic cations estimated from the bionic GHK equation were plotted against ion size as in Fig. 1 B and fit to the hydrodynamic relationship:

$$\frac{P_x}{P_{Na}} = k\left(1 - \frac{d_{ion}}{d_{pore}}\right)^2,$$

where P_x/P_{Na} is the relative permeability of the cation being tested, d_{ion} is the diameter of the test cation, and d_{pore} is the minimal pore diameter. The relative permeabilities for the organic cations were determined from changes in reversal potential induced by replacing extracellular Na^+ in the standard DVF solution with the test cation.

To analyze the voltage dependence of block of Na^+-I_{CRAC} by $Ca^{2+}{}_o$, the model described by Guo and Lu (2000) was used. Unlike the older Woodhull (1973) model that assigns the voltage dependence of block solely to the valence of the blocking particle, the Guo and Lu (2000) model expresses voltage dependence in terms of an apparent valence, an empirical factor that encompasses the effects of blocker valence and the coupled movements of conducting ions displaced by blocker binding.

In this scheme, Ca^{2+} block is described in terms of second-order binding to a single site:

$$Ca_o + Ch \underset{k_{-1},\, z_{-1}}{\overset{k_1,\, z_1}{\rightleftharpoons}} Ch\text{-}Ca \xrightarrow{k_2,\, z_2} Ch + Ca_i$$

(Scheme 1)

where Ch is the channel, $Ca^{2+}{}_o$ and $Ca^{2+}{}_i$ are extracellular and intracellular Ca^{2+}, k_1 and k_{-1} are the binding and unbinding rates from the extracellular side, k_2 is the unbinding rate from the intracellular side, and each z_i represents the apparent valence for the corresponding transition. Block from the intracellular compartment is assumed to be negligible because of low (nanomolar) intracellular Ca^{2+} concentrations. With these assumptions, the fraction of unblocked current is given by (Guo and Lu, 2000):

$$\frac{I}{I_o} = \left\{1 + \frac{[Ca]}{\left(1 + \frac{k_2}{k_{-1}} e^{\frac{-(z_{-1}+z_2)FV}{RT}}\right) K_1 e^{\frac{Z_1 FV}{RT}}}\right\}^{-1}, \quad (1)$$

where $K_1 = k_{-1}/k_1$ is the equilibrium dissociation constant at 0 applied voltage, and Z_1 and z_i are the apparent valences. Z_1 (= $z_1 + z_{-1}$) provides a measure of the overall voltage dependence of Ca^{2+} block and arises from the movement of the charged blocker (Ca^{2+}) within the field as well as the possible displacement of permeant ions (Na^+) within the pore. k_2/k_{-1} is the ratio of the rates of Ca^{2+} escaping into the cytoplasm versus returning to the extracellular solution from the pore, and thus provides a measure of Ca^{2+} permeation. The quantities k_2/k_{-1} and $z_{-1} + z_2$ were treated as single adjustable parameters for fitting the data. To avoid complications arising from activation of Na^+-I_{CRAC} during hyperpolarizing steps in 2-APB–gated channels (see Fig. S2), we measured block from the ratio of the steady-state currents in the presence and absence of extracellular Ca^{2+}, rather than from the ratio of the steady-state to peak currents in Ca^{2+} as was done previously (Prakriya and Lewis, 2006; Yamashita et al., 2007).

T. Begenisich (University of Rochester, Rochester, NY) provided the program that we used to calculate current–voltage relations from a four-barrier, three-site Eyring rate model (Begenisich and Cahalan, 1980; Dang and McCleskey, 1998). In this model, the rate at which an ion moves from one site to another equals the product of the rate constant for this transition and the probability of occupancy of the source site by that ion. The individual rate constants are governed by the barrier heights and well depths. Current for a given ion is determined from the net ion flux rate over the second energy barrier (rate constant × probability of occupancy of that state). The details of the model have been previously described (Dang and McCleskey, 1998). The energies of the binding sites and wells in the model are adjustable parameters and were determined or constrained by known data. These values are justified in the Discussion and indicated in Fig. 9. The extracellular and intracellular Na^+ concentrations were set to 150 mM, extracellular Ca^{2+} was 20 mM, and the intracellular Ca^{2+} concentration was zero in the model.

Online supplemental material

Fig. S1 shows the current–voltage relationships of WT and mutant (E81D, E85A/D87A/E89A, and E165A) Orai3 currents in a 20-mM Ca^{2+} Ringer's solution. Fig. S2 shows the slow activation of the Na^+-CRAC current in DVF solution during hyperpolarizing steps to −100 mV. Fig. S3 shows the power spectrum analysis of Orai3 currents gated by STIM1 or 2-APB. Online supplemental material is available at http://www.jgp.org/cgi/content/full/jgp.201311108/DC1.

RESULTS

Orai3 channels can be activated in a store-dependent manner by the ER Ca^{2+} sensor STIM1 or directly in a store-independent manner by high doses of 2-APB. In contrast to STIM1-activated Orai3 channels, however, 2-APB–activated Orai3 channels exhibit low Ca^{2+} permeability and readily conduct Cs^+ ions (Schindl et al., 2008; Zhang et al., 2008; Yamashita et al., 2011). Here, we sought to understand differences in the interaction of conducting ions to the pores of STIM1- and 2-APB–activated Orai3 channels and compare their gating

behaviors. To carry out these studies, we expressed CFP-Orai3 either alone or together with unlabeled STIM1 in HEK293 cells and studied their functional properties by patch-clamp electrophysiology. STIM1-activated Orai3 currents were obtained by depleting ER Ca^{2+} stores in cells expressing STIM1 and CFP-Orai3 with 1 µM thapsigargin before patch-clamp recordings, whereas 2-APB–activated currents were elicited by administering 2-APB to cells overexpressing CFP-Orai3. A dose–response experiment indicated that 2-APB activates Orai3 channels with an EC_{50} of ~24 µM and a high Hill coefficient of ~8 (Fig. 1 A). Therefore, unless otherwise indicated, we used a concentration of 50 µM to elicit 2-APB–gated Orai3 currents.

Differences in the affinity of Ca^{2+} blockade of Na^+ flux cannot explain the differing Ca^{2+} selectivity of 2-APB– and STIM1-gated Orai3 channels

Unlike STIM1-activated Orai3 channels, 2-APB–gated Orai3 channels readily conduct many large cations (Schindl et al., 2008). In accordance with previous results postulating that an enlarged pore is responsible for this feature (Schindl et al., 2008), 2-APB–activated Orai3 channels display a wider apparent pore width compared with STIM1-activated Orai3 channels (Fig.1 B). As a result of (or associated with) this structural change, 2-APB–gated Orai3 channels exhibit lower Ca^{2+} selectivity than STIM1-gated channels. This is reflected in the well-described leftward shift of the reversal potential (V_{rev}), which changed from 71 ± 6 mV (n = 7) for STIM1-gated channels to 25 ± 2 mV (n = 8) for 2-APB–gated channels in a Ringer's solution containing 20 mM Ca^{2+}. 2-APB–gated Orai3 channels also showed large outward currents carried by intracellular Cs^+ (Fig. 1 C). Moreover, replacing extracellular Na^+ with choline, a large cation that is impermeable through most cationic channels, revealed significant Na^+ conduction at −100 mV (Fig. 1 D), reaffirming that 2-APB–gated channels are poorly Ca^{2+} selective under these experimental conditions.

Current models postulate that the high Ca^{2+} of CRAC channels originates from tight binding of Ca^{2+} to the CRAC channel selectivity filter (Prakriya and Lewis, 2003; Prakriya, 2009; McNally and Prakriya, 2012). On this basis, the widely different Ca^{2+} selectivities of STIM1- and 2-APB–activated channels should arise from differences in the energetics of Ca^{2+} binding to the Orai3 selectivity filter. We examined this question using several approaches: by estimating the thermodynamic stability of Ca^{2+} binding to the Orai3 channel pore from Ca^{2+} block measurements, from the voltage dependence of Ca^{2+} block, and from the rates of Ca^{2+} blockade of the monovalent current. Like voltage-gated Ca^{2+} channels, Orai channels readily conduct a variety of small monovalent cations including Na^+ upon removal of extracellular divalent cations. Therefore, we first applied a DVF solution to elicit Na^+ currents through Orai3 channels and examined the ability of micromolar concentrations of extracellular Ca^{2+} to block the Na^+ currents (Fig. 2).

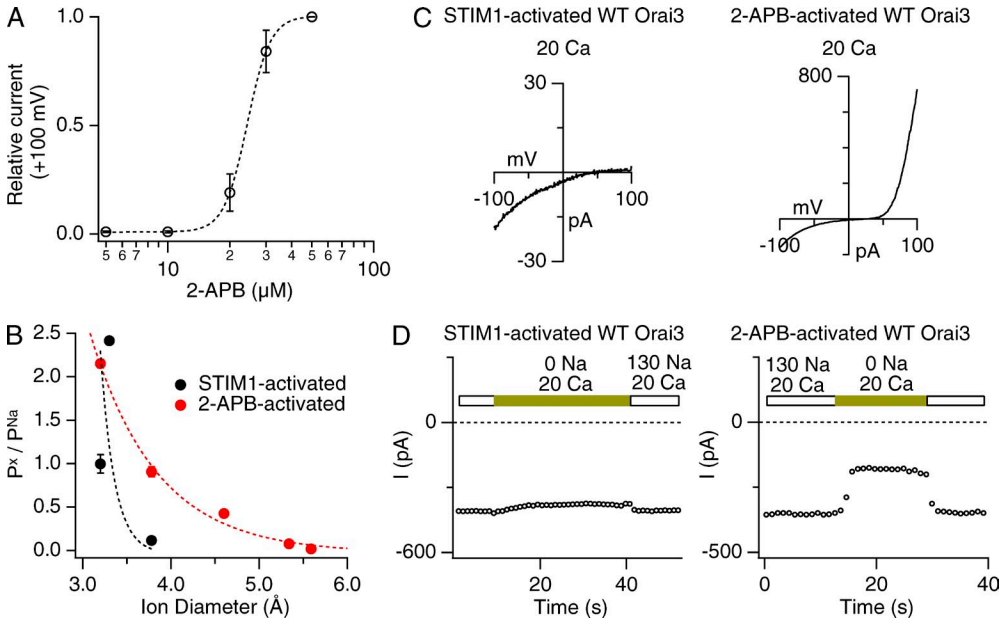

Figure 1. Ca^{2+} selectivity and pore diameter of STIM1- and 2-APB–gated Orai3 channels. (A) Dose dependence of Orai3 activation by 2-APB. 2-APB–gated currents were measured during ramps from −100 to +100 mV, and the current at +100 mV was plotted against the [2-APB]. The dashed line is a fit of the standard Hill equation $I = 1/[1 + (K/[2\text{-APB}])^n]$, with the following parameters: K = 24.3 µM and n = 7.7. Error bars represent SEM. (B) 2-APB–activated Orai3 channels exhibit a wider pore diameter than STIM1-activated channels. Data points reflect the relative permeabilities (P_x/P_{Na}) of organic cations of increasing size. Dashed lines are fits to the hydrodynamic relation (see Materials and methods). Estimated pore diameters from the fits are 3.8 Å (STIM1-activated channels) and 5.6 Å (2-APB–activated channels). (C) I–V relationships of STIM1- and 2-APB–activated Orai3 channels in the presence of 20 mM of extracellular Ca^{2+}. STIM1-activated currents show inwardly rectifying I–V with a positive reversal potential. 2-APB–gated Orai3 channels, in contrast, exhibit an outwardly rectifying I–V with a reversal potential that is considerably left shifted. (D) Removing extracellular Na^+ diminishes inward current (at −100 mV) in 2-APB– but not STIM1-activated Orai3 currents. Extracellular Na^+ was replaced with an equivalent concentration (130 mM) of choline$^+$.

At a membrane potential of −100 mV, these tests indicated that Na^+ currents through STIM1-gated Orai3 channels are blocked dose dependently by extracellular Ca^{2+} with an K_i of ∼25 µM (Fig. 2, A and F). This K_i is nearly identical to the sensitivity of native CRAC channels (Bakowski and Parekh, 2002; Su et al., 2004; Prakriya and Lewis, 2006) and Orai1 channels overexpressed in HEK293 cells (Yamashita et al., 2007). Thus, when gated by STIM1, the thermodynamic stability of Ca^{2+} binding is similar in Orai1 and Orai3 channels, as expected given the high homology of the primary sequence in the pore regions of these paralogous proteins. Furthermore, as previously described for Orai1 channels (Prakriya et al., 2006; Yamashita et al., 2007), mutating the predicted selectivity filter formed by the conserved amino acid Glu81 to Asp (E81D) lowered both Ca^{2+} block (Fig. 2, B and F; K_i = 111 µM) and the Ca^{2+} selectivity of STIM-activated Orai3 channels (Fig. S1 A), as expected if Ca^{2+} selectivity is directly regulated by Ca^{2+} binding at the selectivity filter.

Given that 2-APB–activated Orai3 channels are poorly Ca^{2+} selective, we hypothesized that these channels should be less sensitive to Ca^{2+} blockade than STIM1-gated Orai3 channels. Yet, much to our surprise, Na^+ currents through 2-APB–activated Orai3 channels were blocked with similar Ca^{2+} sensitivity as STIM1-activated channels (Fig. 2, D and F; and Table 1). Moreover, as with STIM1-gated Orai3 channels, blockade of the monovalent current in the 2-APB gating mode was markedly lowered by the E81D mutation (Fig. 2, E and F; and Table 1; K_i = 154 µM), indicating that a pointed disruption of the Ca^{2+} selectivity filter formed by E81 destabilizes Ca^{2+} binding in both gating modes. Introducing the E165A mutation in the TM3 segment of Orai3 did not significantly alter the sensitivity of Ca^{2+} blockade (Fig. 2 F) or Orai3 selectivity (Fig. S1, A and B), effectively ruling out a contribution for E165 and TM3 for Ca^{2+} binding to the 2-APB–activated Orai3 pore. Collectively, these results indicate that the affinity of Ca^{2+} binding to the Orai3 pore at the test potential used here (−100 mV) is not different between the two gating modes, despite the lower Ca^{2+} permeability of 2-APB–gated channels (Fig. 1 D).

Extracellular Na^+ concentration modulates sensitivity of Ca^{2+} blockade of 2-APB–gated Orai3 channels

In many types of ion channels, the sensitivity and rate of open-channel block is affected by the concentration of permeant ions, either because of competition between

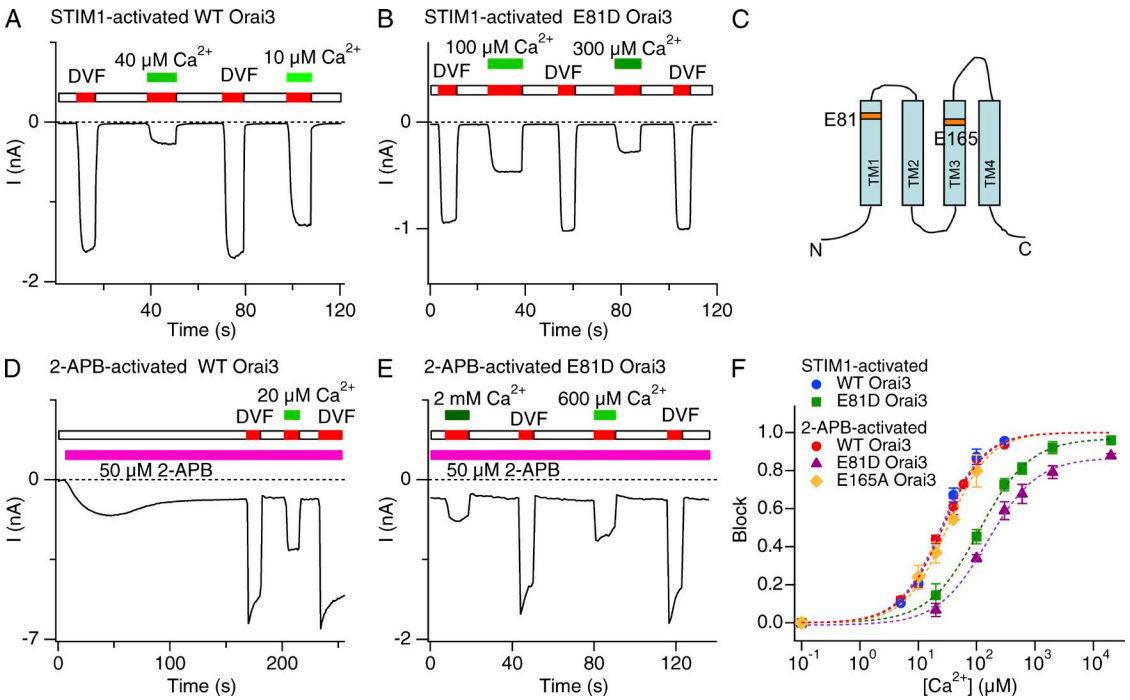

Figure 2. Extracellular Ca^{2+} blocks STIM1- and 2-APB–activated Orai3 Na^+ currents with similar sensitivity. (A, B, D, and E) Inhibition of STIM1- or 2-APB–activated Orai3 Na^+ currents by Ca^{2+}_o. In each case, the cell was voltage clamped to a constant potential of −100 mV and 200-ms sweeps were collected at 2 kHz. The mean current during each sweep is plotted against time. (C) Predicted topology of a single Orai3 subunit with the acidic residues (TM1 and TM3) highlighted. (F) Dose–response relationships of Ca^{2+} blockade. Ca^{2+} blockade of Na^+ currents through 2-APB–activated WT and E165A Orai3 channels occurred with a similar affinity as STIM1-activated Orai3 channels. E81D substitution increases the K_i of block in both STIM1- and 2-APB–activated modes (also see Table 1). Block was quantified by measuring the Na^+ current immediately after application of a DVF solution supplemented with the indicated $[Ca^{2+}]_o$. Each dashed line is a least-squares fit of the Hill equation $block = max/[1 + (K_i/[Ca])^n]$, where *max* is the predicted maximal blockade at saturating Ca^{2+} concentrations. Error bars represent SEM.

blocker and permeant ions for pore binding sites or displacement of the blocker by permeant ions (Armstrong, 1971; Neyton and Miller, 1988b; Antonov and Johnson, 1999). In addition to revealing putative interactions between permeant ions and blockers in the pore, results from such experiments are often useful to delineate the position of pore sites for blockers and permeant ions (Neyton and Miller, 1988a). To approach this issue, we investigated the effects of varying the external Na^+ concentration on Ca^{2+} blockade of inward Orai3 Na^+ currents. These experiments revealed an interesting difference between STIM1- and 2-APB–gated channels. Lowering the extracellular Na^+ concentration from 150 to 75 mM did not significantly alter the sensitivity of Ca^{2+} blockade of STIM1-gated Na^+ fluxes (Fig. 3 A). In 2-APB–gated channels, however, the K_i of inhibition of Na^+ currents in 2-APB–gated channels was reduced threefold to ~9 µM (Fig. 3 B). Thus, decreasing the Na^+ occupancy of external pore sites by lowering $[Na]_o$ enhances Ca^{2+} binding to its high affinity site. Consistent with this interpretation, the blocking rate also increased twofold at the lower Na^+ concentration (Fig. 3, D and E). These results indicate that competition between Na^+ and Ca^{2+} ions in the pore influences the ability of Ca^{2+} to interact with its high affinity site in 2-APB–gated channels. One possibility is that Ca^{2+} has to dislodge Na^+ ions from pore sites before it gains access to its high affinity site. This competition could occur either at the high affinity Ca^{2+} site (i.e., the selectivity filter) itself or at a more superficial location in the pore.

The outer vestibule of all Orai channels contains acidic residues that have been implicated in La^{3+} binding and that are postulated to facilitate cation accumulation at the mouth of the channel (Fig. 3 F; Yeromin et al., 2006; McNally et al., 2009). To examine the role of these residues for the observed competition between Na^+ and Ca^{2+} ions, we mutated these acidic sites (E85A/D87A/D89A) and tested how this maneuver affects Ca^{2+} blockade. Unexpectedly, these tests revealed that block is considerably more complex in the triple mutant than that observed in WT Orai3 channels. Here, Ca^{2+} block exhibited a double sigmoid dependence on $[Ca^{2+}]_o$ at the normal concentration of $[Na^+]_o$. The double sigmoid block could be well fit with the sum of two Hill equations with K_is of 33 and 1694 µM (Fig. 3 C). I–V relations showed that the reversal potential of the current progressively shifts rightward at high $[Ca^{2+}]_o$ (V_{rev} = 10 ± 1 mV in 600 µM Ca^{2+}, 13 ± 1.5 mV in 2 mM Ca^{2+}_o, and 25 ± 1 mV in 20 mM Ca^{2+}_o) but is unchanged in the lower range of $[Ca^{2+}]_o$ (V_{rev} = 8 ± 1 mV at $[Ca^{2+}]$ of 0–300 µM). Thus, we interpret the double sigmoid behavior as the sum of block at low $[Ca^{2+}]_o$ and mixed Ca^{2+}-Na^+ conduction at high $[Ca^{2+}]_o$. Precisely why Ca^{2+} block and Ca^{2+} conduction are so well separated in this mutant remains unclear and additional studies are required to examine this issue. Nonetheless, the block observed at low $[Ca^{2+}]_o$ permits a test of the Na^+ dependence of this behavior. Reducing external $[Na^+]_o$ to 75 mM eliminated the double sigmodicity of blockade in this mutant and block here could be well fit with a single Hill relation (K_i of ~64 µM). Importantly, the K_i of Ca^{2+} blockade at 75 mM $[Na^+]$ is not smaller than the K_i of blockade at high Na^+ (150 mM; Fig. 3 C), indicating that neutralization of the acidic sites in the vestibule eliminates the dependence of block on the extracellular Na^+ concentration. The most straightforward interpretation of these results is that mutation of the external TM1–TM2 loop acidic residues decreases Na^+ binding and accumulation in the outer vestibule, thereby diminishing competition between Na^+ and Ca^{2+} ions and permitting Ca^{2+} to interact with its high affinity site with equal ease irrespective of the Na^+ concentration. The acidic residues of the outer vestibule thus contribute to the accumulation and binding of Na^+ ions in WT Orai3 channels in the 2-APB–gating mode.

Voltage dependence of Ca^{2+} blockade

As shown in Fig. 1, unlike STIM1-gated channels, 2-APB–activated Orai3 channels are poorly Ca^{2+} selective and display significant outward conduction of intracellular Cs^+ ions at positive voltages. In principle, the outward conduction of intracellular Cs^+ ions could arise if Ca^{2+} blockade of monovalent conduction at positive voltages is weaker in 2-APB– than in STIM1-gated channels. To test this possibility, we measured the voltage dependence of Ca^{2+} blockade in the two gating modes from a series of test potentials in 20 µM Ca^{2+}_o (Fig. 4, A and B). These experiments indicated that Na^+ currents in both

TABLE 1

Parameters of Ca^{2+} blockade of Na^+ Orai3 currents

Channel type	K_i	n	*kon*	*koff*	Unitary current
	µM		$M^{-1}s^{-1}$	s^{-1}	*fA*
Orai3 (STIM1-gated)	25	1.2	4×10^6	33	71
Orai3 (2-APB–gated)	26	1.2	3×10^7	246	283
E81D Orai3 (STIM1-gated)	111	1.0	4×10^5	130	–
E81D Orai3 (2-APB–gated)	154	1.0	–	–	–
E165A Orai3 (2-APB–gated)	32	1.2	–	–	–

–, not determined.

gating modes are blocked by extracellular Ca^{2+} in a voltage-dependent fashion, with negligible block at voltages positive to 0 mV (Fig. 4 D). However, the voltage dependence of Ca^{2+} block of 2-APB–activated channels was markedly steeper, and V_{50} more depolarized compared to STIM1-gated channels (Fig. 4 D). The anomalously high voltage dependence of Ca^{2+} block in 2-APB–gated Orai3 channels (Z_1 = 3.4) cannot be explained exclusively in terms of blocking site location because the required site depth is far greater than that of a single Ca^{2+} (z = 2) moving all the way through the electric field (Woodhull, 1973). Instead, as described previously for K^+ channels (Martínez-Francois and Lu, 2010), the most straightforward explanation is that Ca^{2+} block in this case is coupled to the displacement of permeant Na^+ ions. This conclusion is further supported by a striking shift in the voltage dependence of block in the E85A/D87A/E89A triple mutant, where Na^+ ion binding in the vestibule is expected to be absent. Here, the extent of blockade was essentially invariant in a large range of voltages tested (−120 to −20 mV), but declined gradually between 0 and +100 mV (Z_1 = 0.8; Fig. 4 D). These results indicate that the steep voltage dependence of Ca^{2+} blockade in WT 2-APB–gated Orai3 channels is likely driven by the concurrent movement of Na^+ ions that are pushed into the pore from the outer vestibule. When considered together with the finding that external Na^+ ions affect Ca^{2+} binding to the 2-APB–gated pore (Fig. 3 B), these observations lead us to conclude that Ca^{2+} access to the high affinity site is hindered in 2-APB–gated channels as a result of the occupancy of external pore sites by Na^+ ions. Ca^{2+} can block the pore but has to displace several Na^+ ions into the pore to gain access to its binding site.

In contrast to 2-APB–gated channels, the lack of effect of extracellular Na^+ concentration on Ca^{2+} block in

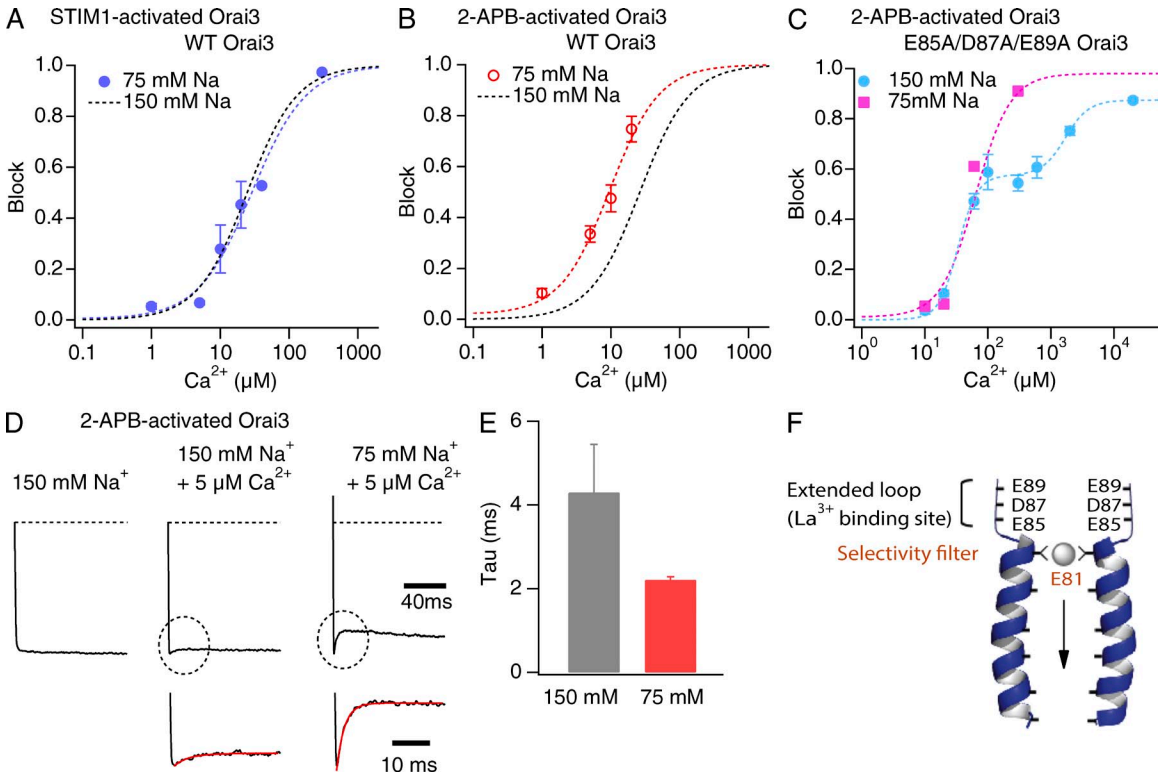

Figure 3. Reducing extracellular Na^+ concentrations affects Ca^{2+} blockade of 2-APB– but not STIM1-gated Orai3 channels. (A and B) Blockade of Na^+ currents through STIM1- or 2-APB–gated channels in 75 mM of external [Na^+]. The dashed line is a least-squares fit of the standard Hill equation $block = max/[1 + (K_i/[Ca])^n]$, where max is the maximal blockade at saturating Ca^{2+} concentrations. The black dotted line in each case is the fit of the data at 150 mM [Na^+] from Fig. 2 F for comparison. Fit parameters for the 75-mM Na^+ condition are: STIM1-activated current, K_i = 29 μM, n = 1.1; 2-APB–activated current, K_i = 9 μM, n = 1.2. (C) Blockade of Na^+ currents through 2-APB–gated E85A/D87A/E89A triple mutant channels at normal (150 mM) and reduced (75 mM) extracellular Na^+. The dashed line in each case is a Hill equation fit with one or two components: $block = max1/[1 + (K_{i1}/[Ca])^{n1}] + (max2 - max1)/[1 + (K_{i2}/[Ca])^{n2}]$, with the following parameters: $max1$ = 0.57, $max2$ = 0.87, K_{i1} = 33 μM, K_{i2} = 1,694 μM, $n1$ = 2.8, and $n2$ = 2.3. The 75-mM Na data were fit with a single Hill equation with a K_i of 64 μM and n = 1.4. (D) The rate of Na^+ current blockade is accelerated by lowering extracellular [Na^+] in 2-APB–gated channels. Traces show the inward Na^+ currents through 2-APB–gated channels during steps to −100 mV. 5 μM of extracellular Ca^{2+} was used to block the Na^+ currents. Inset shows an exponential fit to the initial phase of blockade. (E) Summary of the time constants of Na^+ current blockade by 5 μM $[Ca^{2+}]_o$ ($P < 0.001$). Error bars represent SEM. (F) Schematic representation of the pore-flanking TM1 segments of Orai3 and the acidic residues in the outer pore. The predicted selectivity filter (E81) and the La^{3+} binding sites in the outer vestibule are indicated.

STIM1-gated channels (Fig. 3 A) and the shallower voltage dependence Ca^{2+} block (Fig. 4) suggest that far fewer (if any) Na^+ ions have to be displaced for Ca^{2+} to access its site when the channel is gated by STIM1. This doesn't mean that Ca^{2+} access to its high affinity site is energetically more favorable in STIM1-gated channels; in fact, as described in the next section, the rate constants indicate otherwise. Nonetheless, these results reaffirm the multi-ion nature of the Orai3 pore and are qualitatively consistent with the suggestion that pore occupancy by Na^+ ions is greatly enhanced in 2-APB–gated Orai3 channels than in STIM1-gated Orai3 channels.

Although interesting, the distinct voltage dependencies of STIM1- and 2-APB–gated channels do not readily explain the inability of the 2-APB–gated pore to discriminate between Ca^{2+} and Na^+ ions at negative voltages. This conclusion is supported by at least two aspects of the data. First, at a negative voltage (−100 mV) where STIM1-gated channels are Ca^{2+} selective, 2-APB–gated channels are blocked to a nearly identical extent as STIM1-gated channels, yet the experiments in Fig. 1 clearly show that a large fraction of the current at −100 mV is carried by Na^+. Second and conversely, STIM1-gated channels do not readily conduct monovalent ions (e.g., Cs^+) even at positive voltages (>0 mV), where Ca^{2+} block in these channels is negligible. These characteristics of the voltage dependence indicate that the differing Ca^{2+} selectivities of STIM1- and 2-APB–gated channels cannot be explained directly in terms of the voltage dependence of Ca^{2+} binding to the pore.

The dwell time of Ca^{2+}occupancy is lower in 2-APB–gated channels

In addition to differences in voltage dependence of blockade, STIM1- and 2-APB–activated Orai3 channels showed markedly different kinetics of Ca^{2+} blockade. At −100 mV, STIM1-activated Orai3 currents were blocked by external Ca^{2+} (20 µM) whose initial time course was fit with a single exponential function (Fig. 5, A and B). The time constant of blockade, 7 ± 1 ms (n = 5), closely

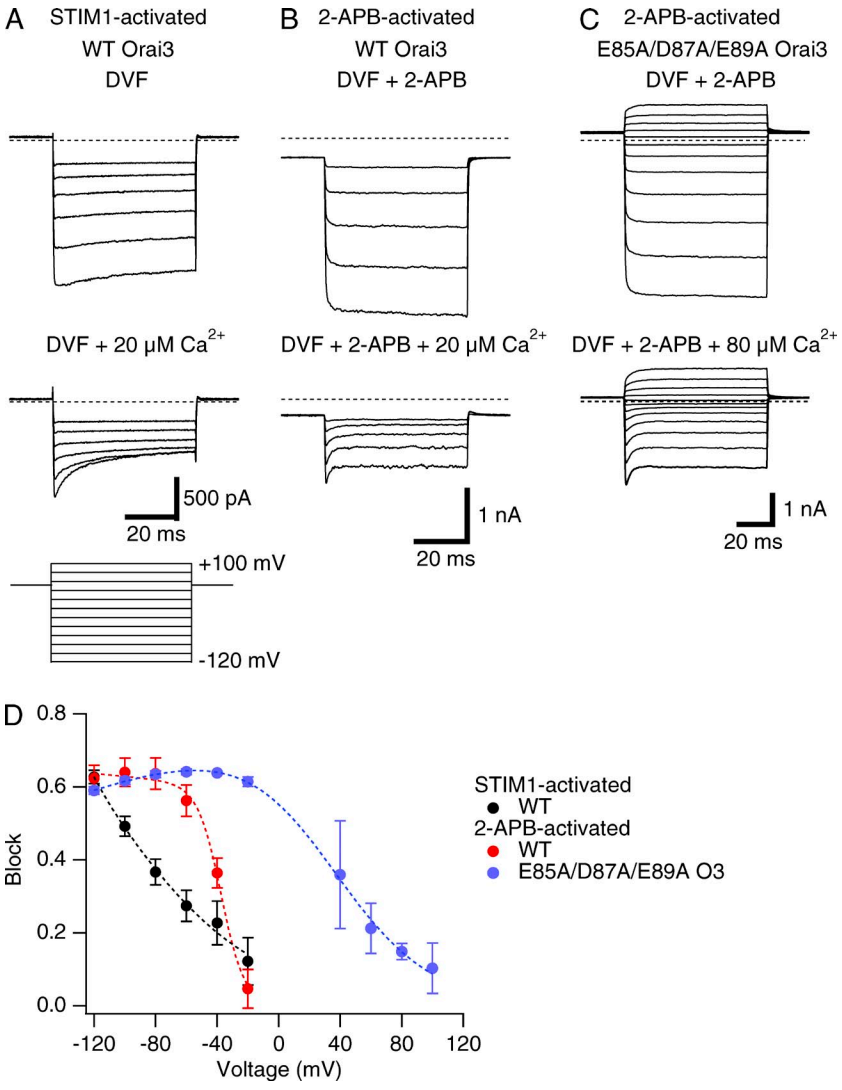

Figure 4. Voltage dependence of blockade of STIM1- and 2-APB–gated Orai3 channels by extracellular Ca^{2+}. (A–C) Effects of extracellular Ca^{2+}_o on Na^+ currents during voltage steps in WT (A and B) or E85A/D87A/E89A mutant (C) Orai3 channels gated by STIM1 or 2-APB. Hyperpolarizing voltage steps from –120 to +100 mV of 50-ms duration were applied from the holding potential (we used holding of +50 mV for STIM1-gated currents and −30 mV for 2-APB–gated currents). Block was induced by either 20 µM Ca^{2+} (STIM1- and 2-APB–gated WT Orai3) or 80 µM (triple mutant). (D) Voltage dependence of Ca^{2+}_o block. Block was quantified from the ratio of the steady-state currents at the end of the 50-ms voltage steps in control and in the presence of extracellular Ca^{2+}_o. The dashed line in each case is a least-squares fit to the Guo and Lu (2000) model (see Materials and methods) with the following key parameters: STIM1-activated Orai3 currents: Z_1 = 0.54, K_1 = 187 µM; 2-APB–activated Orai3: Z_1 = 3.39, K_1 = 4523 µM; 2-APB–gated E85A/D87A/E89A triple mutant: Z_1 = 0.78, K_1 = 9.5 µM. Error bars represent SEM.

matches the block rate previously seen in STIM1-activated Orai1 currents (Yamashita et al., 2007) and native CRAC channels in Jurkat T cells (Prakriya and Lewis, 2006), suggesting that the blocking mechanism is operationally similar in both channel types. For 2-APB–gated channels, measurements of the time constant of Ca^{2+} blockade was complicated by a small degree of slow activation of the monovalent current during steps to −100 mV (Fig. S2). However, lowering the holding potential from +50 to −30 mV diminished the hyperpolarization-induced activation of the 2-APB–gated monovalent current (Fig. S2), allowing us to directly examine the kinetics of Ca^{2+} blockade. These experiments showed that block kinetics were significantly faster in 2-APB–gated channels compared with STIM1-activated channels (Fig. 5, A and B; $\tau = 1.2 \pm 0.1$ ms; $n = 7$ cells).

We used the time constants of Ca^{2+} blockade from these experiments to ascertain the apparent second-order on and off rates of Ca^{2+} binding to the block site. If Ca^{2+} accesses a single binding site from the extracellular side at a rate k_{on} and exits the site at a rate k_{off}, then the time constant (τ) of blockade can be described by the relation:

$$\tau = \frac{1}{\left(k_{on}\left[Ca^{2+}\right] + k_{off}\right)}. \quad (2)$$

Further, the blocked current fraction is given by the relationship:

$$block = \frac{k_{on}\left[Ca^{2+}\right]}{\left(k_{on}\left[Ca^{2+}\right] + k_{off}\right)}. \quad (3)$$

Fig. 5 C plots the reciprocal of the averaged time constant at −100 mV against different Ca^{2+} concentrations. These plots could be well fit with straight lines whose slope represents the apparent second-order on rate constant (k_{on}) and the intercept the off rate constant (k_{off}) for Ca^{2+} binding (Eq. 2). For STIM1-gated channels, the values of these parameters from the fit were $k_{on} = 4 \times 10^6$ $M^{-1}s^{-1}$ and $k_{off} = 33$ s^{-1}. These rate constants are similar to previously measured values for overexpressed Orai1 channels and native CRAC channels in Jurkat T cells (Prakriya and Lewis, 2006; Yamashita et al., 2007), indicating that the rates of Ca^{2+} entry and exit from the selectivity filter do not differ appreciably between STIM1-gated Orai1 and Orai3 channels. In contrast, k_{on} and k_{off} estimated from the data for 2-APB–gated currents were 3×10^7 $M^{-1}s^{-1}$ and 246 s^{-1}, respectively, or approximately eightfold faster than the rate constants for STIM1-activated channels. These substantially faster rate constants imply that the energy barriers for Ca^{2+} entry and exit

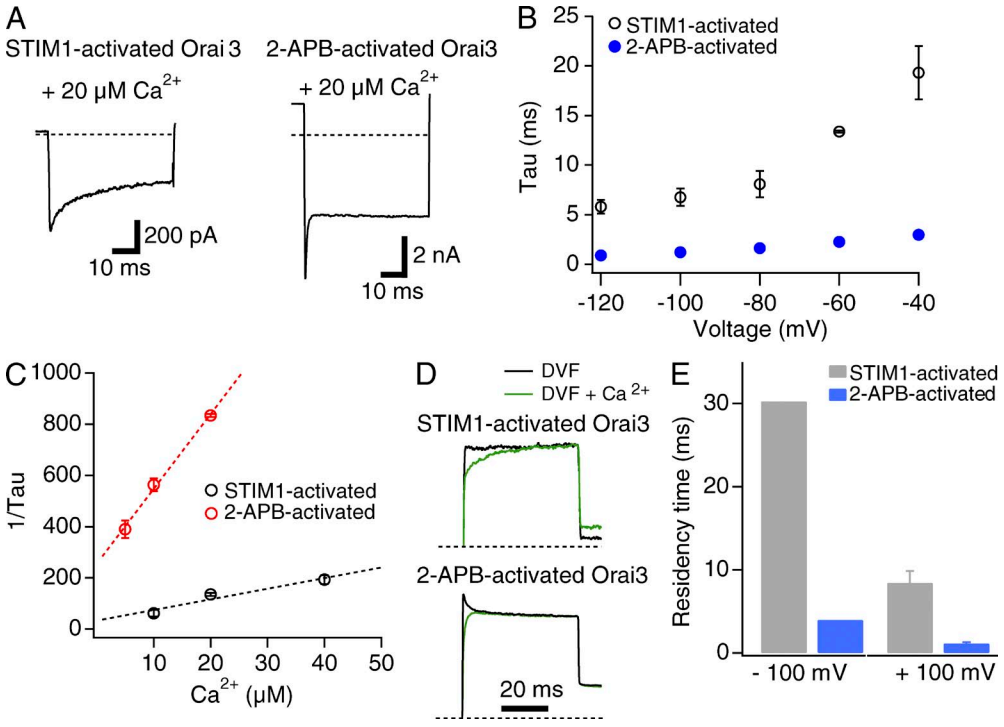

Figure 5. The kinetics of channel blockade is significantly faster in 2-APB–gated channels compared to STIM1-gated channels. (A) STIM1- and 2-APB–activated Na^+ currents in the presence of 20 μM Ca^{2+}. Currents were elicited using a step pulse to −100 mV as described in Fig. 4. (B) Time constants of Ca^{2+} blockade of STIM1- and 2-APB–activated Orai3 currents as a function of voltage. Cells were stepped from the holding potential (+50 mV for STIM1-gated channels and −30 mV for 2-APB–gated channels) to the indicated test pulse. (C) Plot of the reciprocal of the time constant obtained at −100 mV against the blocking Ca^{2+} concentration. The slope and y-axis intercepts of the straight-line fits to the data are 4×10^6 $M^{-1}s^{-1}$ and 33 s^{-1} (STIM1-gated channels) and 3×10^7 $M^{-1}s^{-1}$ and 246 s^{-1} (2-APB–gated channels). (D) Relief from Ca^{2+} block at +100 mV. Ca^{2+} block was induced at 20 μM Ca^{2+}_o through a 200-ms step to −100 mV, and the membrane voltage was stepped to +100 mV to induce relief of blockade. The normalized traces (normalized to the steady-state current at +100 mV) show the recovery from blockade after the step to +100 mV. (E) Summary of the dwell time of Ca^{2+} occupancy at −100 and +100 mV. Dwell times were calculated as $1/k_{off}$. The values at −100 mV were derived from k_{off} estimates from the fit of the mean data shown in C; hence there are no error bars for these values. Data at +100 mV were determined from decay constants in experiments shown in D. Error bars represent SEM.

into/from the pore are lower in 2-APB–gated channels. Further, the faster off rate implies that the dwell time of Ca^{2+} occupancy at the block site ($1/k_{off}$) is significantly lower in 2-APB–activated channels compared with STIM1-activated channels (Fig. 5 E).

In contrast to the acceleration of k_{on} seen in 2-APB–gated Orai3 channels, perturbation of the selectivity filter by the E81D mutation decreased k_{on} tenfold ($k_{on} = 4 \times 10^5\ M^{-1}s^{-1}$ and $k_{off} = 130\ s^{-1}$). This is similar to the previously described behavior of E106D Orai1 mutant channels, which also exhibit substantial slowing of the on-rate constant (Yamashita et al., 2007). Together with the differences in Ca^{2+} block K_i described in Fig. 2, these results indicate that the mechanisms underlying diminished Ca^{2+} selectivity are likely quite different between Orai3 channels gated by 2-APB and E81D Orai3 channels gated by STIM1. Specifically, the lower Ca^{2+} selectivity of E81D Orai3 channels can be rationalized in terms of diminished Ca^{2+} binding to the selectivity filter, in turn related to diminished rate of Ca^{2+} entry into the pore. However, this does not readily explain the lower Ca^{2+} selectivity of 2-APB–gated WT Orai3 channels, which exhibit the same K_i of Ca^{2+} blockade at −100 mV as STIM1-gated Orai3 channels (Fig. 2 E) but accelerated binding rate constants (Table 1). We will return to this issue in the Discussion.

To directly examine unblock kinetics, we depolarized the membrane to +100 mV, where blockade is expected to be nonexistent after induction of block at −100 mV. As shown in Fig. 5 D for STIM1-gated channels, a step to +100 mV initiates current recovery with a time constant of ∼10 ms, reflecting unbinding of Ca^{2+} from the block site. This recovery time specifies a k_{off} (= $1/\tau$) of 100 s^{-1}. Measurements of current recovery in 2-APB–activated channels were complicated by a small degree of deactivation of the control current (i.e., in the absence of blocking Ca^{2+} ions). When channels were blocked by 20 µM Ca^{2+}, however, the deactivation phase was not seen, presumably because it is masked by recovery of current from Ca^{2+} blockade. The time course of current recovery in this phase occurred with a time constant of ∼1 ms. The true current recovery likely occurs with a faster time constant because, as noted above, current recovery in this case would be slowed by channel deactivation occurring simultaneously. Nevertheless, even this overestimated recovery time course specifies a k_{off} of 1,000 s^{-1}, significantly faster than the k_{off} estimate for STIM1-gated channels. Taken together, these results complement findings observed at −100 mV and indicate that Ca^{2+} binding to the 2-APB–gated pore is much more labile than that seen in STIM1-gated channels, and the bound Ca^{2+} comes off at a significantly higher rate.

2-APB– and STIM1-gated Orai3 channels exhibit different sensitivity to La^{3+} blockade

The results presented in Figs. 3 and 4 indicate that Na^+ occupancy at external pore sites is enhanced in 2-APB–gated Orai3 channels relative to STIM1-gated channels. Moreover, tests with the E85A/D87A/E89A triple mutant suggest that this effect is at least partially explained by Na^+ accumulation in the outer vestibule where these residues are positioned. These findings signify that the molecular and structural features of the outer vestibule formed by the TM1–TM2 loops differ in the two gating modes. We examined this issue further by assessing the sensitivity of 2-APB–activated Orai3 channels to blockade by the trivalent lanthanide ion La^{3+}. CRAC channels are potently blocked by low concentrations of lanthanides (Mason et al., 1991; Yeromin et al., 2006). Electrophysiological studies have indicated that high affinity La^{3+} blockade of Orai channels occurs primarily through binding of the trivalent ions to acidic residues in the TM1–TM2 loop segments (Fig. 3 F; Yeromin et al., 2006; McNally et al., 2009). Hence, we rationalized that La^{3+} blockade may allow us to gauge probable alterations in the structure of the TM1–TM2 loops in 2-APB–gated Orai3 channels.

These tests revealed that 2-APB–activated Orai3 channels are significantly less sensitive to La^{3+} blockade than STIM1-activated channels (Fig. 6; apparent K_i = 470 nM in STIM1-gated channels and K_i = 6 µM in 2-APB–gated Orai3 channels, both at −100 mV). Somewhat puzzlingly, the apparent Hill coefficient was also reduced from 1.1 in STIM1-activated currents to 0.7 in 2-APB–activated currents (Fig. 6 C). A Hill coefficient other than 1 is suggestive of multiple binding sites and could arise either because of negative cooperativity between multiple binding sites or progressive occupancy of multiple noninteracting sites with different binding affinities (Prinz, 2010). In the case of Orai channels, although electrophysiological studies indicate that high affinity lanthanide block is explained by blocker binding at the external vestibule (Yeromin et al., 2006; McNally et al., 2009), the recent crystal structure of *Drosophila melanogaster* Orai depicts a Gd^{3+} electron density in close proximity to the Glu selectivity filter in crystals soaked with 1 mM $GdCl_3$ (Hou et al., 2012). Thus, these studies raise the prospect that there are two lanthanide binding sites in the ion conduction pathway: a high affinity site formed by the TM1–TM2 loops, and a second, low affinity site formed by the Glu selectivity filter. Structural alterations in the TM1–TM2 loop residues may reduce but not eliminate high affinity binding entirely, increasing blocker occupancy of the second, low affinity binding site and causing an apparent reduction in the overall Hill coefficient. Consistent with this possibility, mutating the TM1–TM2 loop acidic residues (E85A/D87A/E89A) significantly reduced the sensitivity of La^{3+} blockade, but preserved low affinity blockade. This residual blockade could be well fit with a Hill relation of n = 1 for both STIM1- as well as 2-APB–gated Orai3 channels, which is consistent with the presence of a lower affinity La^{3+} site deeper in the pore. Intriguingly,

the La^{3+} sensitivity of the triple mutant was considerably lower when gated by 2-APB (K_i = 189 µM) than when gated by STIM1 (K_i = 10 µM). Assuming that the residual La^{3+} binding occurs at the selectivity filter (E81), this result reveals that the affinity of ion binding (La^{3+} in this case) at the selectivity filter does in fact differ between 2-APB– and STIM1-gated channels, even though this is not obviously detected in Ca^{2+} at −100 mV (Fig. 2). Based on these observations, we conclude that the TM1–TM2 loops, which form the outer vestibule, adopt a different conformation in 2-APB–gated Orai3 channels, which diminishes La^{3+} binding in the vestibule, but enhances Na^+ occupancy.

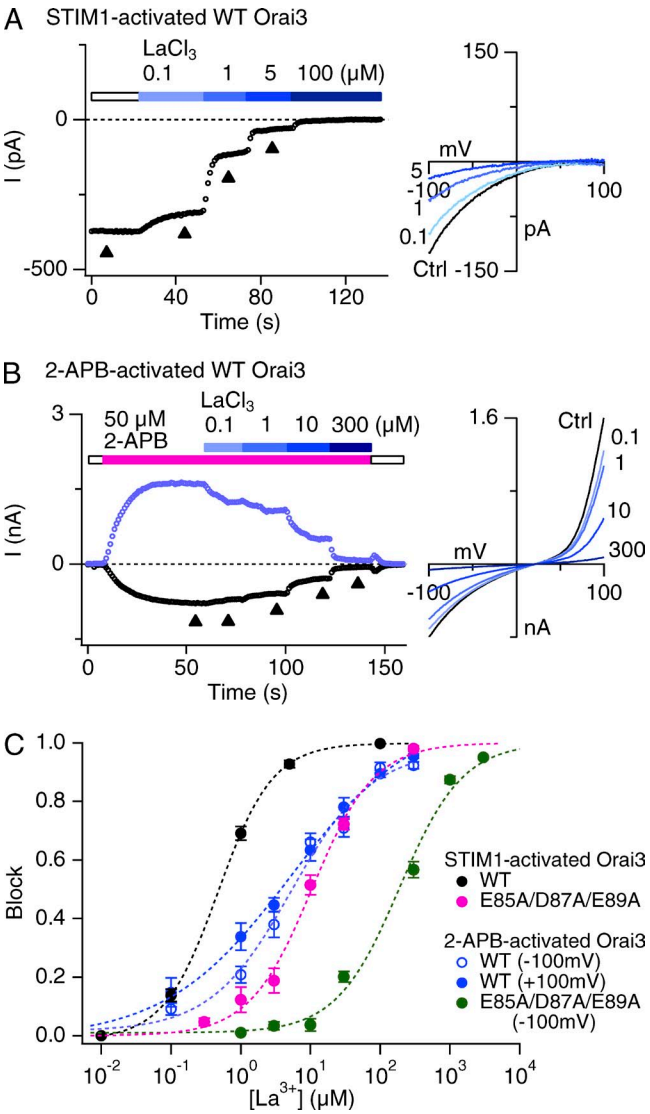

Figure 6. Blockade of STIM1-activated or 2-APB–activated Orai3 current by La^{3+}. (A and B) Currents in 20 mM Ca^{2+}_o through STIM1-gated channels (A) or 2-APB–gated Orai3 channels (B) were blocked with increasing concentrations of La^{3+}. 2-APB–gated currents are depicted at −100 and +100 mV. (C) Dose–response of La^{3+} blockade of STIM1-activated or 2-APB–activated WT and E85A/D87A/E89A mutant Orai3 currents. The dashed lines are least-squares fit to the Hill equation $block = 1/[1 + K_i/(La)^n]$. Each point is the mean ± SEM of four to five cells. Fit parameters are: WT Orai3 + STIM1: K_i = 470 nM, n = 1.1; WT Orai3 + 2-APB: K_i = 6 µM, n = 0.7 (inward current); triple mutant + STIM1: K_i = 10 µM, n = 0.97; triple mutant+2-APB: K_i = 189 µM, n = 0.96.

2-APB–activated Orai3 channels exhibit a higher Na^+ unitary conductance

The faster second-order Ca^{2+} binding rate constants and increased Na^+ ion pore occupancy in 2-APB–gated channels led us to next consider whether the energy barriers for ion flow are diminished in this gating mode. To test this possibility, we estimated the unitary conductance of STIM1- and 2-APB–gated Orai3 channels using nonstationary fluctuation analysis (Sigworth, 1980). Orai3 channels were activated either by 2-APB (50 µM) or by STIM1 after store depletion, and monovalent current noise was analyzed in 200-ms sweeps acquired at −100 mV (Sigworth, 1980). The relationship between current variance (σ^2) and the P_o of the channel can be described by the relation:

$$\sigma^2 = Ni^2P_o(1-P_o), \quad (4)$$

where, i is the unitary current amplitude and N is the number of channels. Eq. 4 indicates that variance is related to P_o by the well-described parabolic relationship, with variance reaching a maximum when P_o is 0.5. Substituting the term for N in terms of the total current ($I = iNP_o$), we get the relation:

$$\frac{\sigma^2}{I} = i(1-P_o). \quad (5)$$

A representative σ^2/I plot of Orai3 current activated by 2-APB is illustrated in Fig. 7 B. The data show that Orai3 channel activation increases σ^2 as expected. Yet, the σ^2 versus I plots did not show a curvature expected from the canonical parabolic σ^2/I relationship. Instead the data could be well fit with straight lines with a mean slope of 56 ± 6 fA (n = 12 cells; Fig. 7 B). As described previously (Prakriya and Lewis 2006), a linear σ^2/I relationship can arise either because channel P_o is always <<1 when the macroscopic current changes because of an increase in P_o (Eq. 5) or, alternately, because of a change in channel number N at any constant value of P_o (Eq. 4). To distinguish between these possibilities and properly interpret the linear σ^2/I relation, an estimate of P_o is needed. For this, we used blockade of Orai3 currents by micromolar concentrations of extracellular Ca^{2+} to define the position along the parabolic σ^2/I relationship where Orai3 channels operate.

If 2-APB activates Orai3 channels to a $P_o > 0.5$, then partial blockade of current with a channel blocker should result in an increase in current variance, as the variance-mean current plot moves leftward on the parabolic σ^2/I plot. Only after further blockade, when P_o is

attenuated to values <0.5, should variance be expected to decline. Consistent with this prediction, modest blockade of the monovalent current by a relatively low dose of extracellular Ca^{2+} resulted in increase in current noise (Fig. 8 A). In contrast, strong blockade at higher Ca^{2+} concentrations decreased current variance. This result indicates that the 2-APB–activated current has a $P_o > 0.5$. In fact, estimates of P_o, i, and N from fits of the data similar to that illustrated in Fig. 8 B revealed values of P_o = 0.7 ± 0.05, i = 283 ± 61 fA, and n = 21,444 ± 4,521 (n = 4 cells). Power spectrum analysis of control and Ca^{2+}-blocked traces indicated that no high frequency components of current noise were missed under the 10-kHz low-pass filtering conditions used for these recordings (Fig. S3 B). These results indicate that 2-APB–activated Orai3 channels have a high P_o.

Measurements of STIM1-gated Orai3 channel variance revealed that these channels also have a high P_o (Fig. 8, C and D). Estimates of P_o, i, and N from fits of the data similar to that illustrated in Fig. 8 D revealed values of P_o = 0.73 ± 0.03, i = 71 ± 1 fA, and n = 22,537 ± 5,670 (n = 5 cells). Power spectrum analysis revealed that STIM1-gated currents exhibit lower frequency noise components than 2-APB–gated currents (Fig. S3), suggesting that despite a similar P_o, 2-APB–gated channels exhibit flickery openings. Importantly, the estimated unitary current of STIM1-gated channels was significantly smaller (71 fA) than unitary current of 2-APB–gated channels (~280 fA).

These results indicate that in the absence of extracellular blocking divalents, 2-APB–gated channels exhibit a significant increase (fourfold) in the rate of Na^+ conduction compared with STIM1-gated channels, which is indicative of a substantial decrease in the energy barriers for Na^+ ion conduction. Moreover, the high P_o and linear σ^2/I plots seen for both 2-APB as well as store-operated Orai3 channels indicate that both modes of activation (at least in the time scales of the 200-ms voltage sweeps used here) occur through a mechanism involving stepwise recruitment of channels to a high P_o mode, rather than a monotonic increase in P_o. This suggests that the gating mechanisms in both modes of channel activation may be operationally similar.

DISCUSSION

In the prevailing model of CRAC channel selectivity, high Ca^{2+} selectivity is achieved through preferential binding of Ca^{2+} at the channel selectivity filter formed by a ring of Glu residues, causing occlusion of Na^+ flux through the pore (McNally and Prakriya, 2012). Central to this idea is the notion that selectivity is governed by high affinity of Ca^{2+} binding to the selectivity filter. In agreement with this possibility, a previous study found that mutation of the selectivity filter (E106D Orai1) results in parallel decreases in both Ca^{2+} selectivity and the affinity of Ca^{2+} blockade of Na^+ fluxes (Yamashita et al., 2007), as would be expected if the strength of Ca^{2+} binding directly influences the ability of bound Ca^{2+} ions to impede Na^+ flux. Such a thermodynamically driven view of Ca^{2+} selectivity predicts that channels with lower relative Ca^{2+} selectivity should display diminished Ca^{2+} blockade of Na^+ flux. Yet, here we find that at a voltage (−100 mV) where 2-APB–gated channels exhibit significant monovalent conduction, inhibition of Na^+ Orai3 current by micromolar concentrations of extracellular Ca^{2+} is similar between the Ca^{2+}-selective STIM1-gated and the nonselective 2-APB–gated Orai3 channels. This result indicates that equilibrium blockade of Na^+ flux, as measured by K_i of Na^+-CRAC inhibition, cannot account for the differing Ca^{2+} selectivity of the two gating modes.

Several explanations can, in principle, be considered for the different Ca^{2+} selectivity of STIM1- and 2-APB–gated channels. One explanation is that selectivity is

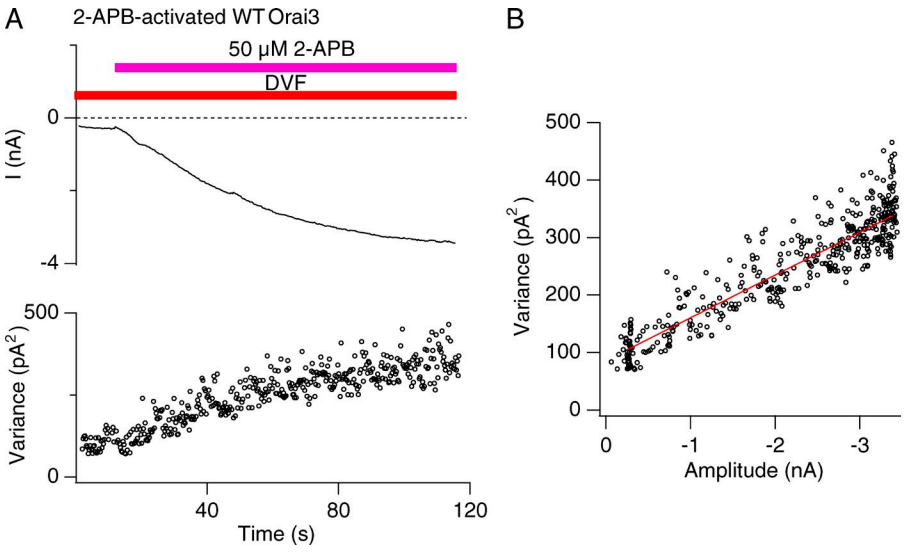

Figure 7. Noise analysis of 2-APB activation of Orai3 currents. (A) The mean current (I) and variance (δ^2) during Orai3 channel activation by 2-APB (50 µM). Na^+ currents in DVF solution activated by 2-APB were measured during 200-ms sweeps at a constant potential of −100 mV. (B) Variance analysis of the 2-APB–activated WT Orai3 Na^+ current from the experiment shown in A. The data are well fit by a line with slope of 77 fA.

influenced not only by the steady-state Ca^{2+} binding affinity to the selectivity filter but also by the kinetic properties of ion entry. Many studies have considered the idea that selectivity is governed by the rates of ion entry into the channel, with less selective channels exhibiting slower rates of ion entry into the selectivity filter (Grabe et al., 2006; Nimigean and Allen, 2011). Applying this idea to Orai3 channels, one scenario is that the weakly Ca^{2+}-selective 2-APB–gated Orai3 channels exhibit a slower rate of Ca^{2+} entry into the high affinity binding site than the highly Ca^{2+} selective STIM1-gated channels. This appears to the case for E81D Orai3 mutant channels, which exhibit a 10-fold slower k_{on} (10^5 $M^{-1}s^{-1}$), reaffirming the importance of high affinity binding at the selectivity filter for Ca^{2+} selectivity. However, this explanation cannot account for the lower Ca^{2+} selectivity of 2-APB–gated WT Orai3 channels because our estimates of the second-order on rates suggest that k_{on} is actually faster in 2-APB–gated channels ($\sim 10^7$ $M^{-1}s^{-1}$) than in STIM1-gated channels ($\sim 10^6$ $M^{-1}s^{-1}$).

A closely related kinetic possibility is that channels with lower Ca^{2+} selectivity exhibit transient (rather than stable) binding compared with channels with high Ca^{2+} selectivity. Indeed, estimates of Ca^{2+} dwell times extrapolated from the k_{off} measurements indicate that 2-APB–gated channels exhibit considerably shorter dwell times than STIM1-gated channels. If this is also true at millimolar concentrations of extracellular Ca^{2+} where Ca^{2+} permeation occurs (which admittedly is an unsubstantiated assumption), the decreased dwell time of Ca^{2+} occupancy could lead to diminished Ca^{2+} selectivity by allowing a higher level of net Na^+ permeation between Ca^{2+} binding events at the block site. Because each bound Ca^{2+} ion would be severalfold slower to leave in STIM1-gated channels, it could prevent many more Na^+ ions from passing through than in 2-APB–gated channels. However, it is also possible that the decreased Ca^{2+} block dwell time is a consequence of enhanced Na^+ permeation driven by repulsion from Na^+ ions destabilizing Ca^{2+} binding (Fig. 3 B). In this case, a faster entry rate for Na^+ would naturally bias selectivity toward Na^+.

A third possibility is that the CRAC channel pore contains additional Ca^{2+} binding sites distinct from the single block site examined here. In this scenario, new Ca^{2+} binding sites that are not readily detected at low (micromolar) concentrations of extracellular Ca^{2+} used to gauge block come into play at millimolar concentrations to confer high Ca^{2+} selectivity of STIM1-gated channels. This argument is undermined by the fact that molecular and structural studies reveal only a single locus for Ca^{2+}

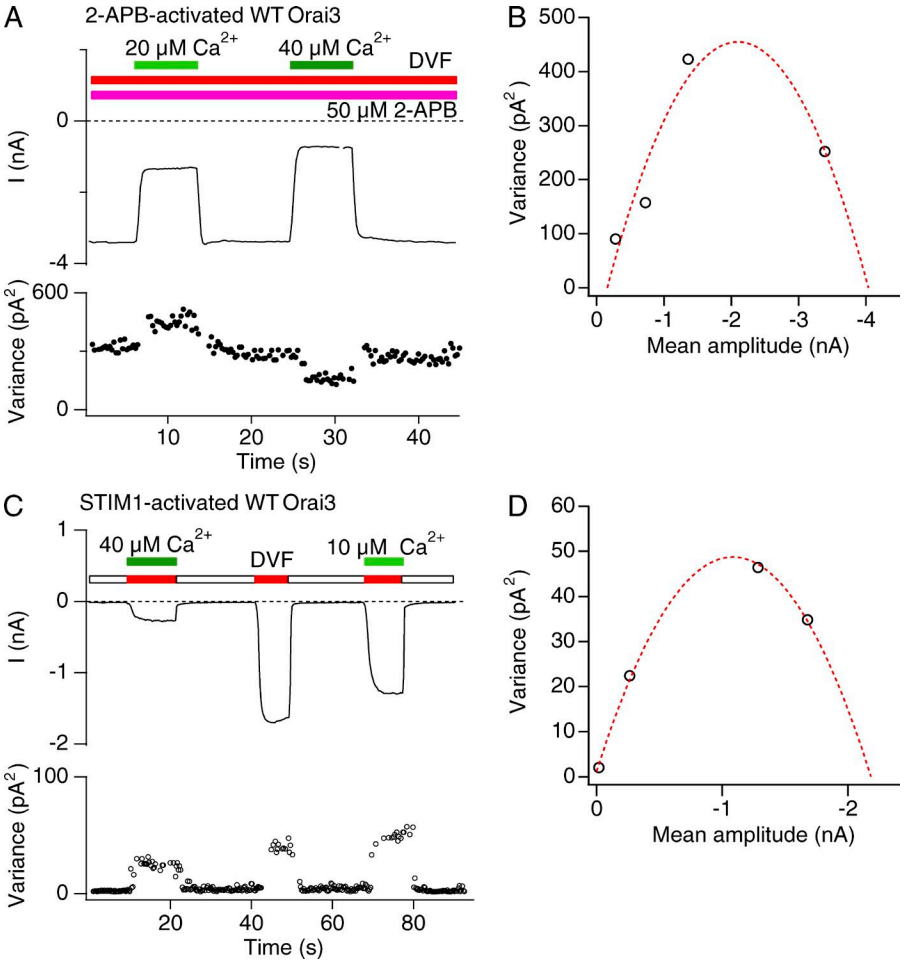

Figure 8. Estimates of the P_o of 2-APB– and STIM1-activated monovalent Orai3 currents. (A) Noise analysis of 2-APB–gated Orai3 currents. The cell was held at a constant potential of −100 mV and different concentrations of $[Ca^{2+}]_o$ were applied in the presence of 50 μM 2-APB to block 2-APB–activated Na^+ currents. The plots show the changes in the mean current (I) and the current variance δ^2 during the experiment. (B) The P_o of CRAC channels activated by 2-APB is >0.5. Current variance from the experiment shown in A is plotted against the mean current. The dashed line is a fit of equation $\delta^2 = Ni^2P_o(1 - P_o)$ with i = 445 fA and n = 10,000 channels. Given these values, the estimated P_o in the absence of Ca^{2+} is 0.83. (C) Noise analysis of STIM1-activated Orai3 currents. Na^+-Orai3 currents were blocked by the indicated concentrations of extracellular Ca^{2+} in thapsigargin-treated cells in DVF solution. (D) The P_o of Orai3 CRAC channels activated by STIM1 is >0.5. The point at I = 0 shows the background variance of the leak current in 20 mM Ca^{2+} + La^{3+}. The dashed line is a fit of equation $\delta^2 = Ni^2P_o(1 - P_o)$ with i = 88 fA and n = 25,000 channels. Given these values, the current in the absence of $Ca^{2+}{}_o$ (DVF) specifies a P_o of 0.77.

binding in the pore composed of conserved Glu residues in TM1 (E106 in Orai1 and E81 in Orai3). The reminder of the pore (TM1) is lined with hydrophobic and basic residues that are not supportive for Ca^{2+} binding. However, a key limitation of the current study is the experimental disconnect between permeability measurements, which can only be performed at high (millimolar) Ca^{2+} concentrations and Ca^{2+} block measurements, which are performed at low (micromolar) Ca^{2+} concentrations. This disconnect is exemplified by the vast difference in Ca^{2+} affinities seen at low and high extracellular Ca^{2+} concentrations: the K_d of Ca^{2+} blockade of Na^+ flux is ~20 µM, but saturation of I_{CRAC} occurs at millimolar Ca^{2+} concentrations (K_m = 1–3 mM; Hoth and Penner, 1993; Premack et al., 1994; Fierro and Parekh, 2000). In fact, this is a common theme in many classes of ion channels: as multi-ion occupancy of the pore increases at high ionic strengths, the apparent affinity of Ca^{2+} binding to the pore declines (Hille 2001), likely through repulsive interactions between closely spaced ions in the pore. One plausible scenario through which this could occur is if the side chains of the six Glu residues in TM1 cluster into two groups along the axis of the pore to form two binding sites. Because these sites would be in close proximity, electrostatic repulsion between the closely spaced Ca^{2+} ions could reduce the apparent affinity of Ca^{2+} binding at the selectivity filter (Almers and McCleskey, 1984; Sather and McCleskey, 2003), potentially explaining the much lower dependence of I_{CRAC} on extracellular Ca^{2+}.

A final possibility is that the change in selectivity arises directly as a consequence of a change in the charge/volume ratio because of structural enlargement of the pore. Some models of Ca^{2+} selectivity have concluded that Ca^{2+} selectivity in L-type voltage-gated Ca^{2+} channels is driven by a charge/space competition mechanism wherein selectivity arises from a balance of electrostatics and the excluded volume of ions in the crowded selectivity filter (Nonner et al., 2000; Sather and McCleskey, 2003; Malasics et al., 2009). Ca^{2+} is selected over Na^+ because its higher charge more effectively neutralizes the negative charge within the narrow confines of the selectivity filter than the monovalent charge of Na^+ ions. These models predict that squeezing the volume of the selectivity filter by narrowing the pore should generally result in preference for Ca^{2+} over Na^+ ions. Conversely, increasing the pore size (as seen in the 2-APB–gated channels) should result in greater monovalent occupancy because of relaxation of the excluded volume and space/charge constraints. Such a model is certainly qualitatively consistent with our experimental observations and more work is needed to illuminate the extent to which volume exclusion and the higher charge/size ratio contributes to Ca^{2+} selectivity in CRAC channels.

Energetics of Ca^{2+} binding

To get an initial understanding of how alterations in the energetics of ion conduction influence Ca^{2+} selectivity, we considered a simple barrier model of the pore based

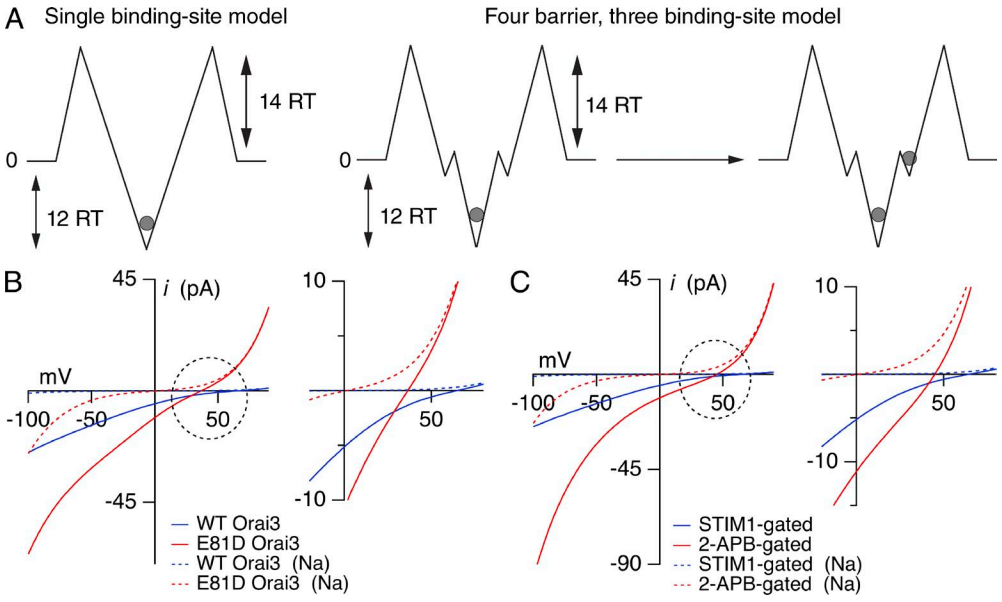

Figure 9. Analysis of the energetics of Ca^{2+} block and permeation using Eyring rate theory. (A) Cartoons depicting a two-barrier, single-site model that was used for analysis of block and a four-barrier, three-site model used for analyzing permeation. The energies of the major barriers and well depths are indicated in RT units. For the four-barrier model, the external barrier heights and deep well energies are identical to those used in the single site model. Energy parameters are as follows: barriers: 14, 2, 2, 14 (Na^+); 14, 2, 2, 14 (Ca^{2+}); wells: 0, −1.5, 0 (Na^+); −0.5, −12.0, −0.5 (Ca^{2+}). The positions of the wells (in electrical distances from the outside) are 0.15, 0.2, and 0.3. (B) I–V relationships of currents in WT Orai3 and E81D STIM1-gated Orai3 channels determined from the four-barrier, three-site model. The energy of the central well was decreased to 9 RT units for E81D Orai3 channels, to account for the decreased K_i of Ca^{2+} block in this mutant. The inset on the right shows the leftward shift in V_{rev} caused by decline in the Ca^{2+} block affinity. Dotted lines indicate the proportion of current carried by Na^+ ions. (C) I–V relationships of STIM1- and 2-APB–gated Orai3 currents. The central well (12 RT units) was identical in the two cases, but the outer barriers were lowered from 14 to 11 RT units for 2-APB–gated channels to account for the increased on/off rates and the larger unitary Na^+ current of these channels. Inset shows the leftward shift in V_{rev} caused by this change. Other parameters were unchanged.

on Eyring rate theory. Rate theory descriptions of the pore in which the ion conduction pathway is depicted as a series of discrete energy wells separated by barriers that limit ion conduction have been widely used to understand the major forces that regulate selectivity and conduction in ion channels (Begenisich and Cahalan, 1980; Hille, 2001). Such models admittedly have limitations in their ability to capture the molecular attributes of the pore such as locations and chemistry of binding sites and the physical basis of energy barriers (Hille, 2001). Nonetheless, they often yield useful insights on the energetic influences of binding sites and barriers and can provide qualitative forecasts of the effects of their changes on ion selectivity. We first considered the simplest model possible: a two-barrier, one binding site model to examine blockade of Na^+ ions by micromolar concentrations of Ca^{2+}. The Gibbs free energy of the Ca^{2+} site can be calculated from the relation:

$$G_{Ca} = RTlnK_d. \quad (6)$$

Substituting the observed values of K_i at −100 mV (Table 1), the relationship specifies a well depth of 11–12 RT units (depending on the extracellular Na^+ concentration) for the Ca^{2+} site. G_{Ca} declines to 9 RT units in the E81D Orai3 mutant channels (K_i of ∼110 µM).

The rate at which an ion moves from one site to another equals the product of the rate constant for this transition and the probability of occupancy of the source site by that ion. For the energy profile diagrammed in Fig. 9 A, the rate constant k_1 is given by:

$$k_1 = ve^{-G/RT}, \quad (7)$$

indicating that entry rate declines exponentially with increasing barrier height. v represents the maximum possible reaction rate set by the thermal vibrational frequency and has the value of 5.8×10^{12} s^{-1} at room temperature ($v = kT/h$, where k is the Boltzmann constant and h is the Planck's constant). For STIM1-gated channels, if the second-order k_{on} is approximated as the rate of Ca^{2+} entry into the pore, then the energy of this transition is given by relation:

$$G = RTln\frac{k}{v}, \quad (8)$$

yielding an outer barrier height of ∼14 RT. Thus, a Ca^{2+} ion lodged at the well faces a total energy barrier of 12 + 14 = 26 RT units to escape back outside. To estimate the height of the cytoplasmic barrier, we used k_{off} estimated from the single-site model (33 s^{-1}). Under our experimental conditions (V_m = −100 mV), if we assume that this is due escape of Ca^{2+} into the intracellular compartment, this rate specifies an energy of 26 RT units, reflecting the total energetic barrier faced by Ca^{2+} ions lodged at the binding site. Thus, the height of the inner barrier is 26 − 12 or 14 RT units, roughly identical to the external barrier. The values of k_{on} and k_{off} increase to 3×10^7 $M^{-1}s^{-1}$ and 246 s^{-1}, respectively, in 2-APB–gated channels. From Eq. 8, these correspond to energies of 12 and 24 RT units for the entry and exit of Ca^{2+} ions from the binding site. Thus, barrier heights for Ca^{2+} decline by roughly 2 RT units in 2-APB–gated channels compared with STIM1-gated channels.

Energetics of Ca^{2+} permeation

The single-site model yields Ca^{2+} unbinding rates (33 s^{-1} in STIM1-gated channels and 245 s^{-1} in 2-APB–activated channels) that are vastly lower than the Ca^{2+} flux rates observed at millimolar extracellular Ca^{2+} concentrations (∼11,000 s^{-1} calculated from a unitary current of ∼3.7 fA at −80 mV [Zweifach and Lewis, 1993]). This paradox, well described in voltage-gated Ca^{2+} channels (Sather and McCleskey, 2003), indicates that single-site models cannot model permeation of Ca^{2+} at high Ca^{2+} concentrations. We therefore considered a four-barrier three-site model similar to the one previously described for voltage-gated Ca^{2+} channels with a single high affinity binding site flanked by two low affinity sites, allowing occupancy of the pore by multiple ions (Dang and McCleskey, 1998). Like voltage-gated Ca^{2+} channels (Sather and McCleskey, 2003), CRAC channels exhibit two Ca^{2+} affinities—a relatively high affinity of 25 µM (−11 RT units) for Ca^{2+} blockade of Na^+ currents (Su et al., 2004; Prakriya and Lewis, 2006; Yamashita et al., 2007) and a low affinity (we used a value of 3.3 mM or −6 RT units [Hoth and Penner, 1993]) for saturation of the Ca^{2+} current. Thus, as extracellular Ca^{2+} is raised from micro- to millimolar concentrations, the apparent affinity of the pore declines by several orders of magnitude, ensuring that ions are not permanently trapped in the pore. In studies of voltage-gated Ca^{2+} channels, this change has been modeled as arising either because of electrostatic repulsion between two closely spaced Ca^{2+} ions located at the selectivity filter (Almers and McCleskey, 1984; Friel and Tsien, 1989) or because of the presence of multiple shallow, low affinity sites flanking a single high affinity site (Dang and McCleskey, 1998), conferring in effect a staircase of multiple rising steps at the exits of the free-energy profile. We used the latter model to evaluate whether changes in barrier heights influence the relative Ca^{2+} selectivity of CRAC channels.

Values of the barrier heights (∼14 RT units) and the central well depth (∼12 RT units) were kept close to estimates in the single-site model. The validity of these energies for the high Ca^{2+}_o condition was confirmed from analysis of the rates of permeation at high Ca^{2+} concentrations. At high (millimolar) Ca^{2+} concentrations under which Ca^{2+} permeation occurs, the off rate for Ca^{2+} conduction is $k_{off} = k_{on} \times K_M$. Substituting the values of k_{on} (4×10^6 $M^{-1}s^{-1}$) and K_M (3.3 mM) yields a k_{off} of ∼12,000 ions s^{-1}. This rate is very close to the

observed flux rate of ions from the unitary Ca^{2+} current amplitude determined from noise measurements (~3–4 fA at −80 to −100 mV, or ~11,000 s^{-1}; Zweifach and Lewis, 1993; Prakriya and Lewis, 2002), indicating that the k_{on} estimate obtained from the single-site model provides a reasonable rate of Ca^{2+} entry into the pore even at high Ca^{2+} concentrations. Likewise, a flux rate of 12,000 ions/s corresponds to a total energy barrier of ~20 RT units from Eq. 8. As noted in the previous paragraph, Ca^{2+} flux saturates with a K_M = 3.3 mM, which specifies a well depth of −6 RT units during Ca^{2+} permeation (Eq. 6). With a total energy barrier of 20 RT units from the deepest to the highest point of the energy landscape during Ca^{2+} permeation and an apparent well of −6 RT units, the inner barrier height should be 20 − 6 = 14 RT units, identical to value estimated from the single-site model. We placed the wells toward the extracellular region of the pore (at electrical distances of 0.15, 0.2, and 0.3 units) to account for the known positions of E81 and the TM1–TM2 acidic residues (E85/D87/E89) in the outer vestibule (Fig. 3 F).

For Na^+ ions, the unitary Na^+ currents of STIM1- and 2-APB–gated channels from noise analysis are 0.08 and ~0.3 pA, respectively, corresponding to off-rate energies of 17 and 14 RT units, respectively. Our tests indicate that the Na^+ current saturates with a K_d of ~90 mM (or −2.4 RT units; unpublished data). With the reasonable assumption that this binding is predominantly governed by the selectivity filter, the barrier heights thus can be determined to be ~14 and 12 RT units in STIM1- and 2-APB–gated channels, similar to the values for Ca^{2+}. The major difference in energy profiles experienced by Ca^{2+} and Na^+ is thus the absence of a high affinity central binding site for Na^+.

With these values of barrier heights and well depths, we next computed the I–V profiles using the four-barrier, three-well model (Dang and McCleskey, 1998). For STIM1-gated channels, the simulated I–V profiles qualitatively matched the experimental I–Vs seen in Orai3 channel activated by STIM1 (Fig. 9, B and C). As predicted from the deep well depth and high barriers for ion flow, the I–Vs showed strong inward rectification with V_{rev} at very positive voltages, typical of STIM1-gated Orai channels. The proportion of current carried by monovalent ions was negligible both at negative and positive voltages (Fig. 9 B). Decreasing the well depth by 3 RT units to mimic the diminished Ca^{2+} block affinity of the E81D Orai3 mutant reduced Ca^{2+} selectivity and resulted in greater monovalent permeation as seen experimentally (Fig. 9 B). This latter finding reaffirms the critical importance of the high affinity Ca^{2+} binding site for Ca^{2+} selectivity. Thus, the model qualitatively reproduces many key experimental features of STIM1-activated Orai3 currents.

To understand why the 2-APB–gated channels exhibit lower Ca^{2+} selectivity, we next altered the parameters of the model to mimic those seen in 2-APB–gated channels. Lowering the outer barriers by 3 RT units for both Na^+ and Ca^{2+} ions while leaving the well depths unchanged elicited profound changes in ion selectivity (Fig. 9 C). The theoretical I–Vs revealed a large leftward shift in the V_{rev} and a significant outwardly rectifying monovalent current, in accordance with the properties observed in 2-APB–gated channels. Importantly, the fraction of inward current carried by Ca^{2+} was significantly diminished compared with the model for STIM1-gated channels. A shallower well depth resulted in even less Ca^{2+} selectivity and greater monovalent ion permeation (unpublished data), as seen in the E81D mutant, again reaffirming the importance but not the exclusive role of the high affinity site for Ca^{2+} selectivity. Thus, these findings reveal that in addition to the well-established influence of the well depth, barrier heights are critical determinants of Ca^{2+} selectivity in CRAC channels. In particular, the results indicate that structural changes that produce broad alterations in barrier heights for permeant ions can elicit robust effects on Ca^{2+} selectivity, even if the well depth for Ca^{2+} binding is unchanged. We consider a possible mechanistic basis of this feature in the following paragraph.

Ca^{2+} selectivity in voltage-gated Ca^{2+} channels, which have a relatively large pore, yet are highly selective for Ca^{2+}, has been traditionally viewed as a prime example of selectivity by affinity. In these channels, the high pore affinity for Ca^{2+} (K_i of ~0.7 µM) is believed to form the basis of the physiologically important selectivity of the channels for Ca^{2+} over the more prevalent Na^+ and K^+ ions (Sather and McCleskey, 2003). In CRAC channels, affinity of Ca^{2+} binding (K_i of Na^+ current blockade) is at least 25-fold lower, yet these channels exhibit comparably high Ca^{2+} selectivity, suggesting that CRAC channels achieve selectivity through additional mechanisms. Based on the experimental and modeling results presented in this study, we propose that in addition to specific Ca^{2+} binding, high Ca^{2+} selectivity of CRAC channels may be attributed, at least in part, to the rejection of all ions (both preferred and non-preferred) by high energy barriers. Enhancing the Na^+ and Ca^{2+} flux rates by lowering the entry and exit barriers paradoxically reduces Ca^{2+} selectivity as seen in the 2-APB–gated channels. This may be related to the decreased residence time of Ca^{2+} occupancy at the block site, thereby increasing opportunistic flow of Na^+ ions between block events. Alternately, it could be related to enhanced Na^+ ion entry rates into the pore, which could destabilize Ca^{2+} binding through a knockoff effect. More quantitative and modeling studies are needed to examine the mechanistic underpinnings of this effect, but the results presented in this study provide a basis for testing these and other models.

What is the physical basis of the wells and barriers in the Eyring model? It is straightforward to expect that the high affinity Ca^{2+} binding site is formed by the selectivity

filter, and the superficial cation binding site can also be plausibly assigned to the vestibule acidic residues (E85/D87/D89; Fig. 3 F). As argued above, an inner cation binding site can also be envisioned to arise at high Ca^{2+} concentrations if the carboxylate side chains of the Glu residues at E81 cluster into two groups to form separate binding sites. It is more difficult, however, to envision the physical basis of the energy barriers, which may in fact not have any tangible physical correlate. The outer "barrier" may simply reflect the ease with which ions are dehydrated. The inner barrier may simply arise from a location in the pore where ions pause momentarily before moving to the next energy minimum. Still, these unknowns do not diminish the lessons of the Eyring rate analysis, for they illustrate the plausibility that both kinetic and thermodynamic factors shape Ca^{2+} selectivity of Orai channels.

Biophysical similarity of 2-APB and STIM1 gating

Analysis of current noise indicates that activation of Orai3 channels by 2-APB occurs through a mechanism qualitatively similar to the stepwise recruitment of silent channels to a high P_o mode described for gating of native CRAC channels by store depletion (Prakriya and Lewis, 2006) and activation of Orai3 channels by STIM1 (this study). In both gating modes, channel opening occurs slowly over time scales of seconds and involves recruitment of closed channels to a long-lasting high P_o state (P_o of ~0.7). One simple explanation is that the slow gating mode of Orai channels is a channel intrinsic behavior, independent of the activation stimulus. However, given the strong nonlinearity of 2-APB activation (Hill coefficient of ~8; Fig. 1 A), an alternative possibility is that the abrupt opening of single channels to the high P_o state reflects the concerted action of multiple ligand molecules (two STIM1 molecules per Orai monomer for STIM1-gated channels [Li et al., 2010; Hoover and Lewis, 2011] and at least eight 2-APB molecules per channel for 2-APB–gated channels) that triggers stepwise channel opening. Either way, this operational similarity suggests that despite differences in the permeation and selectivity of open channels, STIM1 and 2-APB both use a similar molecular mechanism for gating the channel, possibly through related transduction mechanisms wherein the steps between ligand binding and pore opening are identical. This scenario is also consistent with a recent suggestion that 2-APB and STIM1 both use a graded activation mechanism to cause pore opening (Amcheslavsky et al., 2013). More studies are needed to elucidate the complete story of the concerted action of STIM1 and 2-APB on channel opening, taking into account the channel stoichiometry and the presence of multiple ligand binding sites on each Orai subunit.

The authors are grateful to Ted Begenisich for providing the computer program for the four-barrier, three-site Eyring rate model and to Ted Begenisich, Jon Sack, Chris Lingle, and Ed McCleskey for helpful consultations during the course of this work.

This research was supported by National Institutes of Health (grant NS057499).

The authors declare no competing financial interests.

Sharona E. Gordon served as editor.

Submitted: 24 September 2013
Accepted: 30 January 2014

REFERENCES

Almers, W., and E.W. McCleskey. 1984. Non-selective conductance in calcium channels of frog muscle: calcium selectivity in a single-file pore. *J. Physiol.* 353:585–608.

Amcheslavsky, A., O. Safrina, and M.D. Cahalan. 2013. Orai3 TM3 point mutation G158C alters kinetics of 2-APB–induced gating by disulfide bridge formation with TM2 C101. *J. Gen. Physiol.* 142:405–412. http://dx.doi.org/10.1085/jgp.201311030

Antonov, S.M., and J.W. Johnson. 1999. Permeant ion regulation of *N*-methyl-D-aspartate receptor channel block by Mg^{2+}. *Proc. Natl. Acad. Sci. USA.* 96:14571–14576. http://dx.doi.org/10.1073/pnas.96.25.14571

Armstrong, C.M. 1971. Interaction of tetraethylammonium ion derivatives with the potassium channels of giant axons. *J. Gen. Physiol.* 58:413–437. http://dx.doi.org/10.1085/jgp.58.4.413

Bakowski, D., and A.B. Parekh. 2002. Monovalent cation permeability and Ca^{2+} block of the store-operated Ca^{2+} current I_{CRAC} in rat basophilic leukemia cells. *Pflugers Arch.* 443:892–902. http://dx.doi.org/10.1007/s00424-001-0775-8

Begenisich, T.B., and M.D. Cahalan. 1980. Sodium channel permeation in squid axons. I: Reversal potential experiments. *J. Physiol.* 307:217–242.

Dang, T.X., and E.W. McCleskey. 1998. Ion channel selectivity through stepwise changes in binding affinity. *J. Gen. Physiol.* 111:185–193. http://dx.doi.org/10.1085/jgp.111.2.185

DeHaven, W.I., J.T. Smyth, R.R. Boyles, G.S. Bird, and J.W. Putney Jr. 2008. Complex actions of 2-aminoethyldiphenyl borate on store-operated calcium entry. *J. Biol. Chem.* 283:19265–19273. http://dx.doi.org/10.1074/jbc.M801535200

Di Capite, J.L., G.J. Bates, and A.B. Parekh. 2011. Mast cell CRAC channel as a novel therapeutic target in allergy. *Curr. Opin. Allergy Clin. Immunol.* 11:33–38. http://dx.doi.org/10.1097/ACI.0b013e32834232b0

Feske, S. 2009. ORAI1 and STIM1 deficiency in human and mice: roles of store-operated Ca^{2+} entry in the immune system and beyond. *Immunol. Rev.* 231:189–209. http://dx.doi.org/10.1111/j.1600-065X.2009.00818.x

Fierro, L., and A.B. Parekh. 2000. Substantial depletion of the intracellular Ca^{2+} stores is required for macroscopic activation of the Ca^{2+} release-activated Ca^{2+} current in rat basophilic leukaemia cells. *J. Physiol.* 522:247–257. http://dx.doi.org/10.1111/j.1469-7793.2000.t01-1-00247.x

Friel, D.D., and R.W. Tsien. 1989. Voltage-gated calcium channels: direct observation of the anomalous mole fraction effect at the single-channel level. *Proc. Natl. Acad. Sci. USA.* 86:5207–5211. http://dx.doi.org/10.1073/pnas.86.13.5207

Grabe, M., D. Bichet, X. Qian, Y.N. Jan, and L.Y. Jan. 2006. K^+ channel selectivity depends on kinetic as well as thermodynamic factors. *Proc. Natl. Acad. Sci. USA.* 103:14361–14366. http://dx.doi.org/10.1073/pnas.0606662103

Guo, D., and Z. Lu. 2000. Mechanism of cGMP-gated channel block by intracellular polyamines. *J. Gen. Physiol.* 115:783–798. http://dx.doi.org/10.1085/jgp.115.6.783

Hille, B. 2001. Ion channels of excitable membranes. Third edition. Sinauer Associates, Inc., Sunderland, MA. 814 pp.

Hogan, P.G., R.S. Lewis, and A. Rao. 2010. Molecular basis of calcium signaling in lymphocytes: STIM and ORAI. *Annu. Rev. Immunol.* 28:491–533.http://dx.doi.org/10.1146/annurev.immunol.021908.132550

Hoth, M., and R. Penner. 1993. Calcium release-activated calcium current in rat mast cells. *J. Physiol.* 465:359–386.

Hoover, P.J., and R.S. Lewis. 2011. Stoichiometric requirements for trapping and gating of Ca^{2+} release-activated Ca^{2+} (CRAC) channels by stromal interaction molecule 1 (STIM1). *Proc. Natl. Acad. Sci. USA.* 108:13299–13304. http://dx.doi.org/10.1073/pnas.1101664108

Hou, X., L. Pedi, M.M. Diver, and S.B. Long. 2012. Crystal structure of the calcium release-activated calcium channel Orai. *Science.* 338:1308–1313. http://dx.doi.org/10.1126/science.1228757

Kilch, T., D. Alansary, M. Peglow, K. Dörr, G. Rychkov, H. Rieger, C. Peinelt, and B.A. Niemeyer. 2013. Mutations of the Ca^{2+}-sensing stromal interaction molecule STIM1 regulate Ca^{2+} influx by altered oligomerization of STIM1 and by destabilization of the Ca^{2+} channel Orai1. *J. Biol. Chem.* 288:1653–1664. http://dx.doi.org/10.1074/jbc.M112.417246

Lewis, R.S. 2011. Store-operated calcium channels: new perspectives on mechanism and function. *Cold Spring Harb. Perspect. Biol.* 3:a003970. http://dx.doi.org/10.1101/cshperspect.a003970

Li, Z., J. Lu, P. Xu, X. Xie, L. Chen, and T. Xu. 2007. Mapping the interacting domains of STIM1 and Orai1 in Ca^{2+} release-activated Ca^{2+} channel activation. *J. Biol. Chem.* 282:29448–29456. http://dx.doi.org/10.1074/jbc.M703573200

Li, Z., L. Liu, Y. Deng, W. Ji, W. Du, P. Xu, L. Chen, and T. Xu. 2010. Graded activation of CRAC channel by binding of different numbers of STIM1 to Orai1 subunits. *Cell Res.* 21:305–315. http://dx.doi.org/10.1038/cr.2010.131

Malasics, A., D. Gillespie, W. Nonner, D. Henderson, B. Eisenberg, and D. Boda. 2009. Protein structure and ionic selectivity in calcium channels: selectivity filter size, not shape, matters. *Biochim. Biophys. Acta.* 1788:2471–2480. http://dx.doi.org/10.1016/j.bbamem.2009.09.022

Martínez-François, J.R., and Z. Lu. 2010. Intrinsic versus extrinsic voltage sensitivity of blocker interaction with an ion channel pore. *J. Gen. Physiol.* 135:149–167. http://dx.doi.org/10.1085/jgp.200910324

Mason, M.J., M.P. Mahaut-Smith, and S. Grinstein. 1991. The role of intracellular Ca^{2+} in the regulation of the plasma membrane Ca^{2+} permeability of unstimulated rat lymphocytes. *J. Biol. Chem.* 266:10872–10879.

McCarl, C.A., S. Khalil, J. Ma, M. Oh-hora, M. Yamashita, J. Roether, T. Kawasaki, A. Jairaman, Y. Sasaki, M. Prakriya, and S. Feske. 2010. Store-operated Ca^{2+} entry through ORAI1 is critical for T cell-mediated autoimmunity and allograft rejection. *J. Immunol.* 185:5845–5858. http://dx.doi.org/10.4049/jimmunol.1001796

McNally, B.A., and M. Prakriya. 2012. Permeation, selectivity and gating in store-operated CRAC channels. *J. Physiol.* 590:4179–4191. http://dx.doi.org/10.1113/jphysiol.2012.233098

McNally, B.A., M. Yamashita, A. Engh, and M. Prakriya. 2009. Structural determinants of ion permeation in CRAC channels. *Proc. Natl. Acad. Sci. USA.* 106:22516–22521. http://dx.doi.org/10.1073/pnas.0909574106

McNally, B.A., A. Somasundaram, A. Jairaman, M. Yamashita, and M. Prakriya. 2013. The C- and N-terminal STIM1 binding sites on Orai1 are required for both trapping and gating CRAC channels. *J. Physiol.* 591:2833–2850.

Muik, M., I. Frischauf, I. Derler, M. Fahrner, J. Bergsmann, P. Eder, R. Schindl, C. Hesch, B. Polzinger, R. Fritsch, et al. 2008. Dynamic coupling of the putative coiled-coil domain of ORAI1 with STIM1 mediates ORAI1 channel activation. *J. Biol. Chem.* 283:8014–8022. http://dx.doi.org/10.1074/jbc.M708898200

Neyton, J., and C. Miller. 1988a. Discrete Ba^{2+} block as a probe of ion occupancy and pore structure in the high-conductance Ca^{2+}-activated K^+ channel. *J. Gen. Physiol.* 92:569–586. http://dx.doi.org/10.1085/jgp.92.5.569

Neyton, J., and C. Miller. 1988b. Potassium blocks barium permeation through a calcium-activated potassium channel. *J. Gen. Physiol.* 92:549–567. http://dx.doi.org/10.1085/jgp.92.5.549

Nimigean, C.M., and T.W. Allen. 2011. Origins of ion selectivity in potassium channels from the perspective of channel block. *J. Gen. Physiol.* 137:405–413. http://dx.doi.org/10.1085/jgp.201010551

Nonner, W., L. Catacuzzeno, and B. Eisenberg. 2000. Binding and selectivity in L-type calcium channels: a mean spherical approximation. *Biophys. J.* 79:1976–1992. http://dx.doi.org/10.1016/S0006-3495(00)76446-0

Park, C.Y., P.J. Hoover, F.M. Mullins, P. Bachhawat, E.D. Covington, S. Raunser, T. Walz, K.C. Garcia, R.E. Dolmetsch, and R.S. Lewis. 2009. STIM1 clusters and activates CRAC channels via direct binding of a cytosolic domain to Orai1. *Cell.* 136:876–890. http://dx.doi.org/10.1016/j.cell.2009.02.014

Peinelt, C., A. Lis, A. Beck, A. Fleig, and R. Penner. 2008. 2-Aminoethoxydiphenyl borate directly facilitates and indirectly inhibits STIM1-dependent gating of CRAC channels. *J. Physiol.* 586:3061–3073. http://dx.doi.org/10.1113/jphysiol.2008.151365

Prakriya, M. 2009. The molecular physiology of CRAC channels. *Immunol. Rev.* 231:88–98. http://dx.doi.org/10.1111/j.1600-065X.2009.00820.x

Prakriya, M., and R.S. Lewis. 2002. Separation and characterization of currents through store-operated CRAC channels and Mg^{2+}-inhibited cation (MIC) channels. *J. Gen. Physiol.* 119:487–507. http://dx.doi.org/10.1085/jgp.20028551

Prakriya, M., and R.S. Lewis. 2003. CRAC channels: activation, permeation, and the search for a molecular identity. *Cell Calcium.* 33:311–321. http://dx.doi.org/10.1016/S0143-4160(03)00045-9

Prakriya, M., and R.S. Lewis. 2006. Regulation of CRAC channel activity by recruitment of silent channels to a high open-probability gating mode. *J. Gen. Physiol.* 128:373–386. http://dx.doi.org/10.1085/jgp.200609588

Prakriya, M., S. Feske, Y. Gwack, S. Srikanth, A. Rao, and P.G. Hogan. 2006. Orai1 is an essential pore subunit of the CRAC channel. *Nature.* 443:230–233. http://dx.doi.org/10.1038/nature05122

Premack, B.A., T.V. McDonald, and P. Gardner. 1994. Activation of Ca^{2+} current in Jurkat T cells following the depletion of Ca^{2+} stores by microsomal Ca2$^+$-ATPase inhibitors. *J. Immunol.* 152:5226–5240.

Prevarskaya, N., R. Skryma, and Y. Shuba. 2011. Calcium in tumour metastasis: new roles for known actors. *Nat. Rev. Cancer.* 11:609–618. http://dx.doi.org/10.1038/nrc3105

Prinz, H. 2010. Hill coefficients, dose–response curves and allosteric mechanisms. *J. Chem. Biol.* 3:37–44. http://dx.doi.org/10.1007/s12154-009-0029-3

Sather, W.A., and E.W. McCleskey. 2003. Permeation and selectivity in calcium channels. *Annu. Rev. Physiol.* 65:133–159. http://dx.doi.org/10.1146/annurev.physiol.65.092101.142345

Schindl, R., J. Bergsmann, I. Frischauf, I. Derler, M. Fahrner, M. Muik, R. Fritsch, K. Groschner, and C. Romanin. 2008. 2-Aminoethoxydiphenyl borate alters selectivity of Orai3 channels by increasing their pore size. *J. Biol. Chem.* 283:20261–20267. http://dx.doi.org/10.1074/jbc.M803101200

Sigworth, F.J. 1980. The variance of sodium current fluctuations at the node of Ranvier. *J. Physiol.* 307:97–129.

Su, Z., R.L. Shoemaker, R.B. Marchase, and J.E. Blalock. 2004. Ca^{2+} modulation of Ca^{2+} release-activated Ca^{2+} channels is responsible for the inactivation of its monovalent cation current. *Biophys. J.* 86:805–814. http://dx.doi.org/10.1016/S0006-3495(04)74156-9

Varga-Szabo, D., A. Braun, and B. Nieswandt. 2011. STIM and Orai in platelet function. *Cell Calcium.* 50:270–278. http://dx.doi.org/10.1016/j.ceca.2011.04.002

Vig, M., A. Beck, J.M. Billingsley, A. Lis, S. Parvez, C. Peinelt, D.L. Koomoa, J. Soboloff, D.L. Gill, A. Fleig, et al. 2006. CRACM1 multimers form the ion-selective pore of the CRAC channel. *Curr. Biol.* 16:2073–2079. http://dx.doi.org/10.1016/j.cub.2006.08.085

Woodhull, A.M. 1973. Ionic blockage of sodium channels in nerve. *J. Gen. Physiol.* 61:687–708. http://dx.doi.org/10.1085/jgp.61.6.687

Yamashita, M., L. Navarro-Borelly, B.A. McNally, and M. Prakriya. 2007. Orai1 mutations alter ion permeation and Ca^{2+}-dependent fast inactivation of CRAC channels: evidence for coupling of permeation and gating. *J. Gen. Physiol.* 130:525–540. http://dx.doi.org/10.1085/jgp.200709872

Yamashita, M., A. Somasundaram, and M. Prakriya. 2011. Competitive modulation of Ca^{2+} release-activated Ca^{2+} channel gating by STIM1 and 2-aminoethyldiphenyl borate. *J. Biol. Chem.* 286:9429–9442. http://dx.doi.org/10.1074/jbc.M110.189035

Yeromin, A.V., S.L. Zhang, W. Jiang, Y. Yu, O. Safrina, and M.D. Cahalan. 2006. Molecular identification of the CRAC channel by altered ion selectivity in a mutant of Orai. *Nature.* 443:226–229. http://dx.doi.org/10.1038/nature05108

Zhang, S.L., J.A. Kozak, W. Jiang, A.V. Yeromin, J. Chen, Y. Yu, A. Penna, W. Shen, V. Chi, and M.D. Cahalan. 2008. Store-dependent and -independent modes regulating Ca^{2+} release-activated Ca^{2+} channel activity of human Orai1 and Orai3. *J. Biol. Chem.* 283:17662–17671. http://dx.doi.org/10.1074/jbc.M801536200

Zweifach, A., and R.S. Lewis. 1993. Mitogen-regulated Ca^{2+} current of T lymphocytes is activated by depletion of intracellular Ca^{2+} stores. *Proc. Natl. Acad. Sci. USA.* 90:6295–6299. http://dx.doi.org/10.1073/pnas.90.13.6295